PSR Report 2238

# MODELING OF TARGETS, BACKGROUNDS AND ATMOSPHERIC TRANSMISSION PATHS FOR SYNTHETIC GENERATION OF INFRARED SCENES

P. M. Moser
M. Hryszko

December 1991

Final Report
Subcontract Number NASC-91-S-004
Contract N62269-91-C-0561

Sponsored by
Navmar Applied Sciences Corporation
Warminster, PA 18974

and

Naval Air Development Center, Code 5013
Warminster, PA 18974

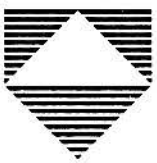

**PACIFIC-SIERRA RESEARCH CORPORATION**
600 Louis Drive, Suite 103 • Warminster, Pennsylvania 18974 • (215) 441-4461
12340 Santa Monica Boulevard • Los Angeles, California 90025 • (213) 820-2200

# REPORT DOCUMENTATION PAGE

*Form Approved*
*OMB No. 0704-0188*



| 1. REPORT DATE *(DD-MM-YYYY)* | 2. REPORT TYPE | 3. DATES COVERED *(From - To)* |
|---|---|---|
| XX-12-1991 | Final Technical | To December 1991 |

**4. TITLE AND SUBTITLE**
Modeling of Targets, Backgrounds and Atmospheric Transmission Paths for Synthetic Generation of Infrared Scenes

**5a. CONTRACT NUMBER**
NASC-91-S-004 and N62269-91-C-0561

**5b. GRANT NUMBER**

**5c. PROGRAM ELEMENT NUMBER**

**6. AUTHOR(S)**
Moser, Paul M.
Hryszko, Mark

**5d. PROJECT NUMBER**

**5e. TASK NUMBER**

**5f. WORK UNIT NUMBER**

**7. PERFORMING ORGANIZATION NAME(S) AND ADDRESS(ES)**
Pacific-Sierra Research Corporation
Warminster, PA 18974

**8. PERFORMING ORGANIZATION REPORT NUMBER**
PSR Report 2238

**9. SPONSORING/MONITORING AGENCY NAME(S) AND ADDRESS(ES)**
Navmar Applied Sciences Corporation
Warminster, PA 18974
and
Naval Air Development Center, Code 5013
Warminster, PA 18974

**10. SPONSOR/MONITOR'S ACRONYM(S)**
NASC
NAVAIRDEVCEN

**11. SPONSOR/MONITOR'S REPORT NUMBER(S)**

**12. DISTRIBUTION/AVAILABILITY STATEMENT**
Approved for public release, distribution unlimited

**13. SUPPLEMENTARY NOTES**
See also "Mathematical Model of FLIR Performance" of 19 Oct 1972 by P. M. Moser (AD-A045247) and related documents: AD-C955799, AD-333365L, AD-D516929L, AD-A045269, AD-A046663, AD-A045248, AD-C012453 and AD-A067731.

**14. ABSTRACT**
The ultimate objective of this project is to develop hardware and software for producing model-based synthetic infrared imagery that will accurately simulate imagery produced by actual forward looking infrared (FLIR) devices and infrared line scanners (IRLS) for these applications: (1) Sensor selection/development/production decisions, (2) FLIR design tool, (3) Sensor evaluation, (4) Tactical mission planning, and (5) Training. In this study, PSR acquired and critically reviewed relevant documents and computer programs relevant to target modeling (with special emphasis on ships), background modeling (with emphasis on sea and sky) and atmospheric transmission modeling. An extensive bibliography is included.

**15. SUBJECT TERMS**
Infrared, Synthetic, Imagery, FLIR, IRLS, Hardware, Software, Simulate, Model-based, FLIR design tool, Mission planning, Sensor development, Sensor evaluation, Training, Ships, Airborne, Sea background, Sky background, Atmospheric transmission

| 16. SECURITY CLASSIFICATION OF: | | | 17. LIMITATION OF ABSTRACT | 18. NUMBER OF PAGES | 19a. NAME OF RESPONSIBLE PERSON |
|---|---|---|---|---|---|
| a. REPORT | b. ABSTRACT | c. THIS PAGE | | | 19b. TELEPHONE NUMBER *(Include area code)* |
| unclassified | unclassified | unclassified | unlimited | 49 | |

# CONTENTS


INTRODUCTION . . . . . 1

MODELING OVERVIEW . . . . . 3

SHIP AND SEA BACKGROUNDS . . . . . 3
- Discussion . . . . . 3
- Modeling Approach . . . . . 5

LAND TARGET AND LAND BACKGROUND MODELS . . . . . 7
- Discussion . . . . . 7
- Modeling Approach . . . . . 8

AIRCRAFT TARGETS AND BACKGROUNDS . . . . . 8
- Discussion . . . . . 8
- Modeling Approach . . . . . 9

ATMOSPHERIC TRANSMISSION MODELING . . . . . 9
- Overview . . . . . 9
- Atmospheric Transmission Models . . . . . 10

CONCLUSIONS . . . . . 15

REFERENCES . . . . . 17

BIBLIOGRAPHY . . . . . 19

FIGURES . . . . . 22-47

# INTRODUCTION

Under Contract N62269-91-C-0561, which was executed on 6 August 1991 with the Naval Air Development Center (NAVAIRDEVCEN), Navmar Applied Sciences Corporation (NASC) is pursuing Phase I of a Small Business Innovation Research (SBIR) project entitled "Synthetic Generation of Dynamic Infrared Scenes." On 16 September 1991, NASC entered into a subcontractual arrangement with Pacific-Sierra Research Corporation (PSR) to provide technical support under Contract NASC-91-S-004.

The ultimate objective of this SBIR project (Topic Description N91-198) is to develop hardware and software for producing model-based synthetic infrared imagery that will accurately simulate the imagery produced by actual airborne forward looking infrared (FLIR) devices and infrared line scanners (IRLS) for the following applications:

Sensor Selection/Development/Production Decisions

An infrared scene generator will enable Navy decision makers to evaluate the worthwhileness of infrared imaging devices versus and/or in conjunction with other sensors, such as night vision goggles, low light television and radar, before embarking on costly development and production programs.

FLIR Design Tool

A dynamic infrared scene generator will enable sensor engineers to perform "what if" experiments before actually designing a new FLIR. For example, in the design of a FLIR, one can trade off spatial resolution for thermal resolution (sensitivity) and thereby arrive at some optimum combination for the particular types and ranges of targets anticipated and for the various environmental conditions. As a second example, why develop a FLIR with resolution good enough to classify a ship at a range of, say, 20 miles if atmospheric water vapor or clouds will limit performance to, say, 5 miles 95% of the time? As a third example, the scene generator will enable one to evaluate comparatively the choice of spectral band (8- to 12.5-μm vs. 3- to 5.5-μm) and also to determine the optimum cut-on and cut-off wavelengths of a selected band (e.g., 8.2- to

12.1-μm) as a function of environmental and operating conditions such as the expected range to the target.

Sensor Evaluation

An infrared scene generator will enable one to extrapolate relatively meager test data from a limited number of test sites to world-wide and throughout-the-year situations. Use of the generator will assist as a data management tool in determining what measurements should be made and their required degree of accuracy and resolution.

Tactical Mission Planning

In an operational situation, an infrared scene generator will enable mission planners to select an optimum mix of weapons and sensors as a function of the environmental conditions existing at the time (or forecast to exist) in the local area of interest; mission participants would be able to "preview" the mission and thereby avoid surprises.

Training

Realistic dynamic simulations of infrared imaging system performance can be used to increase dramatically the breadth and depth of training experiences of airborne operators at a small fraction of the cost of inflight training.

Under its subcontract with NASC, PSR is investigating issues associated with the thermal modeling of targets and backgrounds and with the propagation of radiation emitted and reflected from the scene through the atmosphere to the sensor. NASC is investigating the approaches, both hardware and software, taken by other government and industry establishments in pursuing related synthetic scene generation work, most of which pertains to the visible and microwave portions of the electromagnetic spectrum but which, nevertheless, may be adaptable in a cost-effective manner to the infrared bands. In addition, NASC is addressing the problem of modeling the degrading effects of using a finite sensor on idealized synthetic infrared imagery, taking into account performance-limiting factors such as resolution, sensitivity, noise, and vibration-induced jitter. The findings of the two companies will be coalesced in the preparation of an SBIR Phase II proposal.

# MODELING OVERVIEW

PSR's principal effort in Phase I has been to acquire and critically review relevant documents and computer programs describing prior work and to arrive at conclusions regarding their use, perhaps after modification, in providing synthetic infrared imagery that is, within reasonable limits, qualitatively and quantitatively correct. In the following sections, target modeling (with special emphasis on ships), background modeling (with emphasis on sea and sky backgrounds) and atmospheric transmission modeling are addressed. In addition to a list of references, an extensive bibliography is provided at the end of this report.

# SHIP AND SEA BACKGROUND MODELS

## DISCUSSION

The apparent thermal contrast between a ship and its background is a function of many variables. The actual temperature of its outer surface depends upon the amount of solar energy deposited on the ship, the air temperature, the flow of air past the ship, sea spray, rainfall, and internal heat sources such as the power plant and machinery. Solar heating is the dominant factor in determining ship temperature during the daytime and its influence may persist for several hours after sunset, after which air temperature takes over. The effect of direct solar radiation incident on a ship at any given time is a function of the elevation and azimuth of the sun, atmospheric transmission, cloud cover, and ship heading. In addition, indirect solar radiation, e.g., radiation reflected off the surface of the water and radiation scattered by the clear sky and by clouds contribute to the heat budget of the ship. Because a ship has a large thermal mass, the time history of these factors strongly affects its temperature over a period of several hours. The flow of air past the ship is a function of the speed and direction of both the ship and the wind. Sea spray is a function of sea state and sea direction relative to the ship heading.

The apparent temperature is dependent upon the amount of radiation reflected from the ship. This, in turn, is a function of the intensity and spectral distribution of the incident radiation and of the spectral reflectivity of the paint or other coating (including a possible thin film of water) on the ship.

The ship background may be the sea surface, sky, land, or a combination of these. The reflectivity of smooth sea water varies as a function of viewing angle, ranging from about 2% normal to the surface and increasing slowly to about 6% at an angle of 60° relative to the normal and then increasing to 100% at a grazing angle. However, the sea surface is rarely perfectly smooth and the effect of waves is to reduce the reflectivity. If the surface were perfectly smooth, the sea surface would appear to merge continuously into the sky and one would not be able to see the horizon because the sea would behave as a perfect mirror near the horizon. In reality, because of multiple reflections from waves, the reflectivity increases with angle to a maximum of only about 25% and reaches this peak value at an angle of about 80°.

To an infrared sensor, the apparent temperature of a clear sky varies dramatically with viewing angle, ranging from very low values (of the order of -40°C, depending on wave band) near zenith (in which case the path length through the atmosphere has its minimum value and one is essentially looking out into the void of space), to values close to the air temperature at sea level when one is viewing along a horizontal path through the maximum amount of the most dense part of the atmosphere. Thus, if one is viewing a ship from low altitude over a horizontal line of sight, the ship will be viewed against a sky background of effective temperature that is close to the sea level air temperature.

If the ship is viewed against a sea background, the situation becomes more complicated insofar as what one sees is a combination of radiation emitted by the sea (and therefore characteristic of the sea temperature) and radiation emitted by the sky and reflected off the water. In the daytime, the sea surface would also reflect solar radiation into the sensor. For an opaque body (as is water in the infrared part of the spectrum) the ability of a surface to emit radiation is governed by its absolute temperature (raised to the fourth power) and its *emissivity*, which equals one minus the reflectivity. Thus, for viewing conditions in which the reflectivity is low (e.g., looking straight down at the sea surface), the emissivity is close to its maximum value of one (i.e., about 0.98) and the radiation detected is mostly that *emitted* (rather than *reflected*) by the surface. In such a situation, the apparent temperature of the background against which a ship is viewed is very close to the actual surface temperature of the water. On the other hand, if the ship is viewed under clear sky conditions at an angle of 80° relative to the normal (10° depression angle), the sea background will appear considerably cooler and the ship hull, which might have appeared cool relative to the sea background when viewed vertically, might now appear warm relative to its background. If clouds are present, particularly in the

form of a continuous ceiling of low altitude clouds, the apparent sea surface temperature will be higher but the variation with viewing angle will be much smaller.

Another factor that affects the appearance of a ship is its location relative to the horizon. From geometrical considerations alone, the distance to the horizon (in nautical miles) is equal to 1.06 times the square root of the sensor altitude (in feet). In practice, with an optical device, the horizon extends beyond this value by about 10% because of atmospheric refraction effects - the exact value depending upon the vertical gradient of the index of refraction. If the sensor aircraft is at a low altitude (e.g., 500 ft), the range to the horizon, (24 nmi), could well be less than the range at which the sensor is capable of detecting the target. As a ship goes beyond the horizon, the lower part of the hull begins to disappear first and then, eventually, the superstructure. In some current simulations a flat earth is assumed that extends out to the horizon distance, at which range it abruptly ends and the ship effectively falls off the edge of the earth.

The foregoing serves to illustrate a number of the variables that are associated with the thermal modeling of a ship against a sea/sky background that must be taken into account in a realistic sensor simulation.

## MODELING APPROACH

Initially it will be assumed that the entire ship is at a uniform temperature whose value is governed by the factors identified above. Wilson[1] has developed a procedure called the "Single Element Method" in which the ship is treated as a single vertical element whose temperature is governed largely by environmental conditions; correction factors are then applied to account for internal sources of heat and the different construction of various sections of the ship. Examples of model environmental input parameters are the fraction of clear sky, rainfall rate, wind velocity, the solar constant, and the sun's zenith and azimuth angles. In the Single Element Method, the ship is broken down into sections having common internal temperatures and subsequently into sections having common thermal capacity of its outer walls. A basic thermal element is chosen to be a vertical element of unit surface area and the lowest internal temperature and the lowest thermal capacity of all ship sections. The basic element temperature is calculated and correction factors are derived from the differences of the remaining sections. Correction factors account for the variations in internal temperature and

thermal capacity and for the presence of a hot stack. An equation describing the temperature of the basic element is found from a heat balance on this element.

As previously indicated, the apparent temperature of the ocean surface is a function of many variables including its actual temperature over the first few micrometers of depth, sea roughness, angle of viewing, sun and sky conditions, and wave band over which the sensor is operating. It has been found by Hulburt[2] that the optical properties of the sea surface remain approximately constant as the wind increases from 5 to 25 knots. This may be considered as the normal weather condition at sea. Two other possible conditions are a mirror calm sea and a sea well covered with white caps, as for winds above 30 knots. These conditions are not encountered frequently; however, they can be modeled using Fresnel's equations for reflection off dielectric surfaces for the case of the "glassy" sea and by treating the surface as a diffuse Lambertian reflector for the rough sea case. The foregoing addresses only the *temperature* modeling of the sea surface; modeling texture is a separate issue. Accurate modeling of ocean waves and swell is a task that has stymied oceanographers and hydrodynamicists. A single train of trochoidal waves can be described mathematically; however, if there are many trains of waves of different wavelengths (and therefore exhibiting different celerities) passing in different directions through a given region, the problem becomes intractable, partly because the superposition principle does not hold. That is, the wave amplitudes do not add linearly, and indeed, breaking waves may occur.

It is believed that, initially at least, it would not be cost effective to attempt to model accurately the texture of the sea. However, the effective temperature of the sea could be modelled for the three sea conditions cited above by use of methods developed by Saunders[3]. Unfortunately, Saunders limited his attention to the 8.3- to 12.5-μm (LWIR) band. The situation in the 3.0- to 5.3-μm (MWIR) band is more complicated in that the intensity of sun glitter off the wave facets in the MWIR band is 17 times greater than in the LWIR band while the radiation emitted from a representative target (say, at 15°C) is less than about 1/19 times as great in the MWIR band as in the LWIR band. Stated differently, relative to levels of radiation from targets, sun glitter is more than 300 times as intense in the MWIR band than in the LWIR band.

Figures 1 and 2 are infrared line scanner images that illustrate the effects of sun glitter in the LWIR and MWIR bands respectively. These two pictures of the sail structure of a decks-awash submarine were recorded at about noon in early August off

Block Island, NY. In the LWIR picture the glitter pattern is at a level that is low enough that it can be ignored; in the MWIR picture, however, parts of the glitter pattern are so intense that the target is difficult to find.

Results of modeling the sun-sky background radiance and "bouncing" it off the surface of an idealized ocean by use of Fresnel's reflection equations are illustrated in figure 3, which shows the angular distribution of power for an arbitrary sun zenith angle of 30° and a wavelength of 0.5 μm. For the MWIR band and, even more so, for the LWIR band, the magnitudes of the upwelling radiance will be considerably less than at 0.5 μm although the spatial distributions will be similar.

It is proposed to model sun glitter only in the MWIR band by extending the data of Cox and Munk[4] to that band.

## LAND TARGET AND LAND BACKGROUND MODELS

### DISCUSSION

An extensive body of information exists on thermal modeling of land targets. In general, the target is represented by an assembly of polygonal graybody radiating facets and the effective temperature of each is calculated by considering the heating effects of radiation from the sun, sky and terrain, radiative and convective losses to the surround, and internal heating effects from the consumption of fuel. Heat absorbed during the day is lost at night. The process depends on the thermal heat capacities of the structures constituting the target, and atmospheric conditions such as the degree of overcast and the air temperature. When the humidity is high, the sky is cloud covered, and the air temperature is nearly constant, the scene tends not to vary much from day to night. On the other hand when the weather is clear and cloudless both day and night, large excursions in temperature occur. The effect of a strong wind is to reduce the temperature excursions within the scene and the thermal signature is, in part, "blown away." During and after periods of rainfall the scene tends to become more uniform in temperature and thermal contrasts become "washed out." However, for targets that contain heat sources, background washout may actually be advantageous in reducing the intensity of competing features.

The diurnal variation in effective temperatures of background features may exceed the variations in the targets. For example, an unexercised target of large thermal mass parked on dark, loose, dry sand may vary little in temperature throughout a 24-hour period while the sand temperature varies over many tens of degrees.

### MODELING APPROACH

The foregoing discussion serves to illustrate the number and diversity of parameters that must be involved in modeling of land targets and land backgrounds. Fortunately, there already exists a significant body of information and experience acquired by the Army which should be adaptable to Navy and Marine Corps applications. Army agencies performing such work include the Tank-Automotive Command, the Center for Night Vision and Electro-Optics and the Ballistics Research Laboratory. To avoid duplication of effort, computer programs will be acquired from such organizations and modified as required.

## AIRCRAFT TARGETS AND BACKGROUNDS

### DISCUSSION

Under tri-service sponsorship, Photon Research Associates, Inc. (PRA) has developed three complementary computer codes for modeling infrared scenes associated with aircraft. The Target Signature Simulation (TARSIS) software[5] provides a first-principles method of calculating energy emitted by and reflected from the air vehicle's frame, but does not include plume energy. The simulation requires four inputs: (1) atmospheric description, i.e., attenuation, path radiance, sunshine, earthshine, and skyshine in the vicinity of the target (provided by the APART code), (2) target description, i.e., a facet model for the target vehicle, the temperature of each facet and the paint scheme, (3) sensor description, i.e., spectral bandwidth and response, field of view and resolution, and (4) viewer geometry, i.e., positions of the target, sun and observer. Based on these inputs and on internal data bases describing the paint reflectances, TARSIS calculates the source, apparent, and target/background contrast intensities. These intensities or signatures are available spatially (i.e., for each facet) and spectrally (i.e., as a function of wavelength) and as a function of radiation source. The software has

been designed for rapidly generating sequences of these signatures as range and aspect are varied.

The other two PRA codes are GENESSIS and APART. GENESSIS is used for modeling the background and APART, which is based on LOWTRAN, is used for performing the atmospheric calculations.

### MODELING APPROACH

The TARSIS software is written in ANSI-standard FORTRAN 77. Copies of the code and documentation are available through the Naval Ocean Systems Center.

## ATMOSPHERIC TRANSMISSION MODELING

### OVERVIEW

One of the most crucial issues affecting the accurate prediction of the performance of an infrared imaging device is the modeling of the transmission of infrared radiation through the atmosphere. While modeling of targets and backgrounds may, to a large extent, be concerned with how realistic their simulated images appear, modeling of the atmosphere may govern whether their images appear at all. This issue is of great importance in deciding what infrared band should be selected for a particular application; considerable sums of money could be wasted by a misguided choice.

Attenuation occurs in the atmosphere by absorption and by scattering of radiation. Absorption takes place because certain molecules in the atmosphere (e.g., $CO_2$, $H_2O$, $O_3$) possess electric or magnetic dipole moments which serve as "handles" by which an electromagnetic field can "seize" the molecules and impart to them energy of vibration or rotation at certain allowable frequencies, resulting in a reduction in the energy of the field at those frequencies. At very low pressures, such absorption occurs over very narrow frequency intervals. However, at higher pressures (e.g., atmospheric pressure), because of increased interaction of the molecules at shorter distances and shorter mean times between collisions, this frequency interval broadens and, as a result, the wings of the absorption lines overlap and, depending on the particular constituent, may form a broad-band continuum in addition to the fundamental absorption lines. Water vapor, the most

important and the most variable atmospheric molecular absorber in the infrared, exhibits continuum absorption in addition to spectral line absorption.

Attenuation by scattering results from radiation being redirected from its normal path by particles in the atmosphere and therefore not intercepted by the sensor. The most important scatterers are those particles whose dimensions are larger than or comparable to the wavelength of the radiation. For the infrared bands, aerosols, consisting mostly of water droplets suspended in the air in the form of haze or fog, are the important scatterers. In general, there is a wide distribution of particle sizes within a given haze or fog; furthermore, the shape of the distribution depends upon the type of atmosphere (e.g., maritime, urban, rural, desert). One measure of the aerosol content in the atmosphere is the "daylight visibility range" (often called meteorological range or simply "visibility"). Visibility is defined as the horizontal distance over which the apparent contrast in daylight between two large objects exhibiting 100% contrast is reduced to 2%. Although visibility is defined only for the visible part of the spectrum, it is often extended into the infrared by use of scaling rules that take into account wavelength and the distribution of particle sizes, the latter usually expressed in terms of the type of atmosphere (maritime, rural, etc.).

## ATMOSPHERIC TRANSMISSION MODELS

Absorption of infrared radiation by atmospheric gases has been studied extensively under both controlled laboratory conditions and in the real atmosphere. The Infrared Handbook[6] cites 114 references on the subject and lists an additional 197 publications in a bibliography. Various establishments, notably the Air Force Geophysics Laboratory (AFGL), have sought to filter, purify and distill this enormous body of corporate knowledge in the form of computer codes. AFGL has published models and computer codes that permit calculation of transmission at high spectral resolution (FASCOD2), moderate resolution (MODTRAN) and low resolution (LOWTRAN). In addition, AFGL has prepared HITRAN, which is not a transmission model, but a data base of molecular spectroscopic parameters. Other models in current use are the Photon Research Associates, Inc. Atmospheric Propagation and Radiative Transfer (APART) computer code. The model in most common use is LOWTRAN 7, whose resolution is adequate for modeling thermal imaging devices.

LOWTRAN has been available in its various embodiments for almost twenty years. During that time it has often been criticized for not being perfect and consequently many revisions and improvements have been made. It is generally acknowledged that for moderate water vapor concentrations and moderate path lengths, LOWTRAN works quite well. However, there have been anecdotal reports that LOWTRAN seriously underpredicts performance in the LWIR band particularly for long paths containing large amounts of water vapor. For example, there have been reports of the detection of ships in the Indian Ocean by fleet airborne FLIRs at ranges of the order of 50 to 70 nmi. Unfortunately, quantitative environmental data adequate to permit calculation of expected detection ranges were lacking for the occasion. However, synoptic environmental data used in the then-current version of LOWTRAN indicated a very low probability for detection at such long ranges.

Numerous papers have been published in which LOWTRAN predictions are compared with measured data; however, most of the measured data have been obtained under laboratory conditions with artificial atmospheres and no aerosols present. Data measured over long paths (i.e., over several tens of miles) are quite limited.

In a classic series of experiments, Taylor and Yates[7,8,9] of the Naval Research Laboratory measured atmospheric transmission in the infrared along low-altitude, horizontal paths over Chesapeake Bay ranging in length from 305 m (1000 ft) to 16.25 km (8.8 nmi) and along a nearly horizontal path of length 27.7 km (14.9 nmi) at an average altitude of about 10,000 ft between two mountains on the island of Hawaii.

As an adjunct to the evaluation of infrared imaging equipment developed under the Long Focal Length Imaging Demonstration (LFLID) project, Hess et al.[10] engaged Avco Everett Research Laboratory and OptiMetrics, Inc. to make direct measurements of atmospheric spectral transmittance over a 66.2-km slant path between sites on the islands of Maui and Lanai. Vertical profiles of air temperature and water vapor concentration were derived from radiosonde measurements. Manning, Dowling and Hummel[11] subsequently reported that, although good agreement existed between measured data and LOWTRAN 6 calculations for the MWIR band, LOWTRAN 6 appeared to underpredict LWIR transmittances by factors ranging from about 2 to 4. See figures 4 and 5. After the draft report of Manning et al.[11] had been issued, it appeared that errors had been made in presenting the measured transmittance data, the correction of which made the

disagreement even worse. Hess et al.[12] reported the corrected data, reproduced here as figure 6, which shows that LOWTRAN 6 is pessimistic by as much as a factor of 10.

Resolution of this issue, or at least determining the ranges of parameters over which LOWTRAN is valid, is of special interest in this study. Because of the aforementioned concerns about LOWTRAN, in the Phase I proposal for this project it was proposed that for atmospheric transmission paths containing up to 30 cm of precipitable water, the now-current LOWTRAN 7 model would be used and for paths containing more than 30 cm of precipitable water, the Altshuler[13] model would be used. The Altshuler model has been applied in the past[14] with apparent success for total amounts of water vapor in the target-to-sensor path of up to 100 cm of precipitable water.

The initial approach taken in this study was to compare predictions of LOWTRAN 7 with those obtainable with the Altshuler model to identify potential problems in seamlessly linking the two models. Next, comparisons were made between LOWTRAN 7 and the classic long-path measurements of Taylor and Yates[7,9], and lastly, with the more recent data of Manning et al.[11] and Hess et al.[12]

In the Altshuler model it is assumed that transmission through water vapor can be calculated by use of a single parameter, namely, the total amount of precipitable water vapor in the path. This assumption greatly simplifies performance modeling of infrared sensors. On the other hand, for LOWTRAN 7, attenuation by water vapor depends not only on the total amount of water vapor in the path but also on the concentration of water vapor in the path. In the Altshuler model it doesn't matter, for example, if one has a 10-nmi path containing 2 cm of precipitable water per nmi or a 5-nmi path containing 4 cm of precipitable water per nautical mile. For LOWTRAN 7 the same is true of the attenuation by the water vapor absorption lines but not for the water vapor continuum absorption.

An attempt was made to see if agreement could be obtained between the Altshuler and LOWTRAN 7 models for some reasonable range of amounts of water vapor. Figure 7 shows the spectral transmittance through total amounts of water vapor ranging from 1 to 100 cm of precipitable water obtained by following Altshuler's procedure. LOWTRAN 7 was then normalized to the Altshuler model for the case of 100 cm of precipitable water in the path. It was found that a water vapor concentration of 4.1 $g/m^3$ placed LOWTRAN 7 in agreement with Altshuler for the 100 cm case as shown in

figure 8. Note that, as was to be expected, there is reasonable agreement between the two models for large amounts of water vapor in the path; however, for the smaller amounts, LOWTRAN 7 predicts higher transmittances than Altshuler.

In a second example, a water vapor concentration of 9.5 $g/m^3$ was assigned to LOWTRAN 7 and path lengths were selected to yield the same set of total water vapor amounts as before. The results of this trial are shown in figure 9. LOWTRAN predicts higher transmittances for the cases corresponding to less than 10 cm of precipitable water vapor in the path and lower transmittances for paths containing more than 10 cm of water. Additional discrepancies exist in the peak transmission wavelength. LOWTRAN predicts the peak transmission to occur at 9.5 μm compared to Altshuler's 11 μm. Although it is believed that, if necessary, LOWTRAN 7 could be made to emulate the Altshuler model adequately (for thermal imaging purposes) over limited ranges of the parameters, it has now been concluded that this is not the best of the available approaches.

As part of this Phase I SBIR program a comprehensive review of computer-based atmospheric modeling was performed. The most widely accepted standard for low resolution atmospheric propagation models is LOWTRAN 7. This propagation model and computer code enables the calculation of atmospheric transmittance and background radiance from 0 to 50,000 $cm^{-1}$ at a resolution of 20 $cm^{-1}$. Among other things, it includes new molecular band model parameters that yield higher transmittances in the LWIR band compared with LOWTRAN 6. LOWTRAN 7 provides a useful starting point for atmospheric modeling for this project. However, a potential problem area exists in the LWIR band for moderate to high water vapor concentrations. A continuing investigation will be required to resolve perceived discrepancies between measured data and LOWTRAN 7 before it is implemented in the image train model. It appears at present that the errors may be in the measured data.

The LOWTRAN models have relied heavily on a long history of measurements by Burch and his associates[15,16]. Grant[17] has provided an excellent critical review of the state of knowledge of transmission of 8- to 13-μm radiation through water vapor. Grant points out that the earlier work of Burch et al., which was the basis for the attenuation coefficients associated with the water vapor continuum absorption used in LOWTRAN 6, suffered from several sources of experimental error. In the earlier work of Burch et al. water vapor apparently had condensed on the surfaces of the mirrors used

in the multiple path absorption cell for the cases of high water vapor concentration. In Burch's more recent measurements, the mirrors were heated to prevent condensation, which resulted in a 20% reduction in the measured coefficients. Also, earlier laboratory measurements of absorption by water vapor were performed with nitrogen as the host gas in the absorption cell. It has been found that nitrogen produces a greater broadening of the water vapor absorption lines and, consequently, greater continuum absorption, than if a mixture of oxygen and nitrogen corresponding to the atmosphere is used. The more recent results form the basis for the values used in HITRAN, FASCOD2 and LOWTRAN 7.

In an attempt to determine the degree of agreement between LOWTRAN 7 and data measured over long atmospheric paths, PSR has taken the published data of Taylor and Yates[7,9], Manning et al.[11] and Hess et al.[12] and computed LOWTRAN 7 transmission spectra for the MWIR and LWIR bands, using the environmental data they provided.

Figures 10 through 24 allow comparisons to be made between LOWTRAN 7 results and the experimental data of Yates and Taylor. It is seen that, in most cases, LOWTRAN 7 predicts smaller transmittances, in both the MWIR and LWIR bands, than the values measured by Yates and Taylor. Contrary to previous expectations, there is relatively good agreement for the longer paths of 16.25 km and 27.7 km, especially for the cases of high visibility. For the cases of lower visibility, the disagreements become greater, particularly for the LWIR band where LOWTRAN 7 appears to underpredict by a factor of 2 to 3. One possible reason for the discrepancy is the way that the effects of visibility are scaled from the visible part of the spectrum to the infrared. If the principal reason for poor visibility on a given occasion is a large concentration of aerosols having particle sizes of the order of the wavelength of visible light (e.g., 0.55 μm) but a very small concentration of particles in the size regime of about 10 μm, LOWTRAN 7 could seriously underestimate LWIR transmittances. Kneizys et al.[18] conclude, on the basis of measurements made over 8-km and 2.25-km paths at Wright-Patterson Air Force Base, the data showed good agreement with LOWTRAN 6 calculations, provided the calculations were made under the assumption of no aerosols present for measurements made under conditions of low visibility.

Figures 25 and 26 permit comparison of a small portion of the measured data of Manning et al.[11] with LOWTRAN 6 and LOWTRAN 7 calculations. Figure 27 shows

the vertical profiles of temperature and water vapor concentration in the vicinity around the time of the transmission measurements. The absolute humidity varied from 3 to 14 grams per cubic meter as a function of altitude. Manning et al. show good agreement between LOWTRAN 6 calculations and measured data in the MWIR band but an underprediction by a factor of about 4 for the LWIR band. On the other hand, PSR calculations with LOWTRAN 7, shown also in figures 25 and 26, show good agreement with the measurements in both the MWIR and LWIR bands. Condray[19] has performed a study of LOWTRAN 6 vs. LOWTRAN 7 and concludes that, for high water vapor concentrations, LOWTRAN 6 is more pessimistic than LOWTRAN 7, but for an absolute humidity of 10 $g/m^3$, the difference is only several percent. It is suspected that Manning et al. erred in their LOWTRAN calculations.

Hess et al.[12] have presented a small subset of the Manning et al. data after making a "correction" in the measured transmittance data, increasing those values by a factor of 2.5. This increases the discrepancy to a factor of 10 between the measured values and the LOWTRAN 6 values of Manning et al. Figure 28 is a reproduction of data from Hess et al. and the PSR LOWTRAN 7 calculations for the same set of conditions.

## CONCLUSIONS

A wealth of information exists in the form of documents and computer codes that is relevant to generating synthetic infrared imagery that is, within limits, qualitatively and quantitatively correct. Models covering both the spatial and thermal characteristics of land, sea and air targets have been subjects of intensive development. It appears that the greatest deficiencies occur in modeling extremely variable target backgrounds and environmental conditions. That is, once a particular target type has been established as being of interest, it is a relatively straightforward, although by no means trivial, task to generate a thermal model of it. On the other hand, backgrounds and environmental conditions can exhibit essentially infinite variability.

It appears, from the bibliographic material provided in this report, that from the viewpoint of scene generation, relatively little work has been done in the areas of modeling sea and sky backgrounds. Most of the reference material in these areas consists of basic scientific papers that will have to be applied to models.

It is concluded that, in the area of atmospheric transmission modeling, LOWTRAN 7, with certain qualifications, is the model of choice. It has been recommended[20] that LOWTRAN 7 be used in the modeling calculations but that FASCOD2 also be used for occasional sanity checks to provide correction factors for those cases in which the results from LOWTRAN 7 are questionable. Studies of the sensitivity of results to be obtained from the infrared scene generator to errors in atmospheric transmission calculations should be performed. For example, greater percentage errors could be tolerated over short clear paths (for which atmospheric attenuation is not a significant issue) than over long paths for which the atmosphere could determine whether a target can be detected outside of its defensive envelope.

As shown in this report, LOWTRAN 7 does an amazingly good job of "predicting" measured data. However, for certain situations (e.g., low visibility), departures by a factor of two to three were observed. The interim solution used by some workers has been to delete the effects of aerosol attenuation in their LWIR calculations to obtain a better match. The conclusion is that LOWTRAN 7 should be used, but used with caution.

At the beginning of the Phase II work, a set of guidelines should be established restricting the range of atmospheric conditions under which LOWTRAN 7 should be exercised in the scene generator to those for which its errors cause negligible effects. This will allow the atmospheric model to be used, for example, in comparing performance in the MWIR and LWIR bands. In Phase II, a rigorous investigation and comparison of published experimental results and LOWTRAN 7 calculations should be performed. The previously established bounds of atmospheric water vapor and aerosol conditions will be extended and the final recommendations for the atmospheric portion of the image train model will be reported. The studies will include consideration of both the MWIR and LWIR bands to ensure that transmission in both bands is modeled correctly and that comparisons of performance of the two bands are valid. These efforts will be performed in parallel with other parts of the project.

# REFERENCES


1. D. M. Wilson, "A Method of Computing Ship Contrast Temperatures Including Results Based on Weather Ship J Environment Data," Naval Surface Weapons Center Report NSWC/WOL TR 78-187, 29 Jan 1991

2. E. O. Hulburt, "The Polarization of Light at Sea," Journal of the Optical Society of America **24**, 35 (1934)

3. P. M. Saunders, "Radiance of Sea and Sky in the Infrared Window 800-1200 $cm^{-1}$," Journal of the Optical Society of America" **58**, 645, (1968)

4. C. Cox and W. Munk, "Statistics of the Sea Surface Derived from Sun Glitter," Journal of Marine Research **16**, 198 (1954)

5. Photon Research Associates, Inc. TARSIS Computer Code (Version 7.1) Reference Manual, November 1987

6. W. L. Wolfe and G. J. Zissis, Editors, *The Infrared Handbook*, Environmental Research Institute of Michigan (1985)

7. J. H. Taylor and H. W. Yates, "Atmospheric Transmission in the Infrared," Naval Research Laboratory Report 4759, July 2, 1956

8. H. W. Yates, "The Absorption Spectrum from 0.5 to 25 Microns of a 1000-ft Atmospheric Path at Sea Level," Naval Research Laboratory Report 5033, September 27, 1957

9. H. W. Yates and J. H. Taylor, "Infrared Transmission of the Atmosphere," Naval Research Laboratory Report 5453, June 8, 1960

10. M. R. Hess, W. K. Hull and M. D. Gibbons, "Long Focal Length Imaging Demonstration (U)," Proceedings of the IRIS Specialty Group on Infrared Imaging, January 1984

11. J. L. Manning, J. A. Dowling and J. R. Hummel, "Ship-to-Ship Propagation: Maritime Data Analyses," OptiMetrics, Inc. Draft Report OMI-116, December 1984

12. M. R. Hess, J. Gibbons, J. Toner, W. Abrams, R. Chin, M. Gibbons and M. Winn "The Long Focal Length Imaging Demonstration (LFLID) Project (U)," Proceedings of the Meeting of the IRIS Specialty Group on Infrared Imaging, March 1985

13. T. L. Altshuler, "A Procedure for Calculation of Atmospheric Transmission of Infrared," General Electric Advanced Electronics Center at Cornell University Report R57ELC15, 1 May 1957

14. P. M. Moser, "Mathematical Model of FLIR Performance," Naval Air Development Center Tech Memo NADC-20203:PMM, AD-A045 247, 19 October 1972

15. D. A. Gryvnak and D. E. Burch, "Infrared Absorption by $CO_2$ and $H_2O$," Air Force Cambridge Research Laboratories Report AFGL-TR-0154, AD-A060 079, May 1978

16. D. E. Burch and R. L. Alt, "Continuum Absorption by $H_2O$ in the 700-1200 $cm^{-1}$ and 2400-2800 $cm^{-1}$ Windows," Air Force Geophysics Laboratory Report AFGL-TR-0128, AD-A147 391, May 1984

17. W. B. Grant, "Water vapor absorption coefficients in the 8-13-μm spectral region: a critical review," Applied Optics **29**, 451 (1990)

18. F. X. Kneizys, R. R. Gruenzel, W. C. Martin, M. J. Schuwerk, W. O. Gallery, W. O. Clough, J. H. Chetwynd, and E. P. Shettle, "Comparison of 8 to 12 Micrometer and 3 to 5 Micrometer CVF Transmissometer Data With LOWTRAN Calculations," Air Force Geophysics Laboratory Report AFGL-TR-84-0171, AD-A154 219, 26 June 1984

19. P. M. Condray, "A LOWTRAN7 Sensitivity Study in the 8-12 and 3-5 Micron Bands--Includes Comparisons with LOWTRAN6 Results," USAF Environmental Technical Applications Center Report USAFETAC/TN-90/002, AD-A222 094, February 1990

20. M. E. Thomas, personal communication

# BIBLIOGRAPHY

P. P. Ostrowski and D. M. Wilson, "A Simplified Computer Code for Predicting Ship Infrared Signatures," Naval Surface Weapons Center Report NSWC/TR-84-540, AD-B099 632L, 13 November 1985

M. A. Mazzer, R. J. Mitchell, et al., "Computer Simulation of Warships in the Infrared (U)," Proceedings of IRIS **26**, No. 1, 209, June 1982

P. E. Batley, "Ship Infrared Signatures (SIRS) Computer Model - Technical Overview and User's Manual," Naval Ship Research and Development Center Report SME-78-37 (1978)

R. J. Becherer and G. L. Harvey, "Simplified Models of Ship Infrared Signatures (U)," Proceedings of IRIS **24**, 141, October 1979

D. M. Wilson and B. S. Katz, "Performance of Electro-Optics Systems Against Time-Varying Ship Signatures (U)," Proceedings of IRIS **25**, No. 3, 229, March 1981

G. L. Harvey and R. J. Becherer, "Dynamic Variations of Ship Infrared Signatures," Naval Research Laboratory Report No. EOTPO-51, AD-C019 271L, 17 August 1979

D. Friedman, "Ship Infrared Signature (U)," Naval Research Laboratory Report 7330, AD-518 232L, 15 October 1971

Z. C. Bennett, C. F. Bieber, et al., "The Infrared Radiant Intensity of the USS Gyatt (U)," Naval Research Laboratory Report 6978, AD-505 766L, 15 October 1969

D. C. Burdick, K. D. Ervin, et al., "Interim Assessment of Ships by Infrared (U)," Naval Research Laboratory Memorandum Report 1879, AD-391 152L, 1 May 1969

H. Shenker et al., "Ship Infrared Signatures and Countermeasures (U)," Proceedings of IRIS **15**, No. 2, 225, September 1970

I. Wilf and Y. Manor, "Simulation of sea surface images in the infrared," Applied Optics, **23**, 3174 (1984)

F. Rosell and G. Harvey, Editors, "The Fundamentals of Thermal Imaging Systems," Naval Research Laboratory Report 8311, 10 May 1979

R. D. Chapman and G. B. Irani, "Errors in estimating slope spectra from wave images," Applied Optics **20**, 3645 (1981)

P. M. Saunders, "Shadowing on the Ocean and the Existence of the Horizon," Journal of Geophysical Research **72**, 4643, (1967)

N. Ben-Yosef, B. Rahat, and G. Feigin, "Simulation of IR images of natural backgrounds," Applied Optics **22**, 190 (1983)

O. E. Toler and D. S. Grey, "Simulation model for infrared imaging systems," SPIE **226** Infrared Imaging Systems Technology, 121 (1980)

T. J. Rogne, C. S. Hall, R. Freeling, G. R. Gerhart and D. J. Thomas, "U. S. Army Tank-Automotive Command (TACOM) Thermal Image Model (TTIM)," SPIE **1110** Imaging Infrared: Scene Simulation, Modeling, and Real Image Tracking, 210 (1989)

U. Bernstein, A. Stenger, and B. Kaye, "An IR imaging simulation system," SPIE **1157** Infrared Technology XV, 200 (1989)

N. Ben-Yosef, K. Wilner and M. Abitbol, "Natural terrain in the infrared: Measurements and Modeling," SPIE **819** Infrared Technology XIII, 66 (1987)

R. I. Koda, U. Bernstein and C. E. Todd, "Generic infrared system model with dynamic image generation," SPIE **1110** Imaging Infrared: Scene simulation, Modeling, and Real Image Tracking, 232 (1989)

C. E. Keller, A. J. Stenger and U. Bernstein, "Improved IR image generator for real-time scene simulation," Technology Service Corporation

U. Bernstein and C. E. Keller, "A thermal model for real-time textured IR background simulation," SPIE International Symposium on Optical Engineering and Photonics in Aerospace Sensing," 1-5 April 1991

A. T. Zavodny and M. A. Mazzer, "Simulation of cultural scenes for passive infrared sensors," Technology Service Corporation

S. Jandrall, E. Schweitzer and J. Barrilleaux, "A Tactical Infrared Scene Generator," SPIE **1110** Imaging Infrared: Scene Simulation, Modeling, and Real Image Tracking, 2 (1989)

R. J. Evans and P. M. Crane, "Dynamic FLIR simulation in flight training research," SPIE **1110** Imaging Infrared: Scene Simulation, Modeling, and Real Image Tracking, 11 (1989)

M. E. Thomas, "Infrared- and Millimeter-Wavelength Continuum Absorption in the Atmospheric Windows: Measurements and Models," Infrared Physics, **30**, 161, (1990)

C. T. Delaye and M. E. Thomas, " Atmospheric continuum absorption models," SPIE Vol. 1487 Propagation Engineering: Fourth in a Series ( 1991)

S. A. Clough, F. X. Kneizys, R. Davies, R. Gamache and R. Tipping, "Theoretical Line Shape for $H_2O$ Vapor; Application to the Continuum," Atmospheric Water Vapor, A. Deepak, T. D. Wilkerson and L. H. Ruhnke, Editors, Academic Press, New York (1980)

F. X. Kneizys, E. P. Shettle, W. O. Gallery, J. H. Chetwynd, L. W. Abreu, J. E. Selby, S. A. Clough and R. W. Fenn, "Atmospheric Transmittance/Radiance: Computer Code LOWTRAN 6," Air Force Geophysics Laboratory Report AFGL-TR-0187, 1 August 1983

F. X. Kneizys, E. P. Shettle, L. W. Abreu, J. H. Chetwynd, G. P. Anderson, W. O. Gallery, J. E. Selby and S. A. Clough, "Users Guide to LOWTRAN 7," Air Force Geophysics Laboratory Report AFGL-TR-88-0177, 16 August 1988

A. D. Devir, A. Ben-Shalom, S. G. Lipson, U. P. Oppenheim and E. Ribak, "Atmospheric Transmittance Measurements: Comparison with LOWTRAN 6, Report RAA/99-85, Technion-Israel Institute of Technology, Haifa 32000, Israel (1985)

L. L. Smith, T. Hilgeman and B. Sandford, "Long-Path Airborne Infrared Atmospheric Transmission (U)," Proceedings of IRIS **28**, 193, June 1983

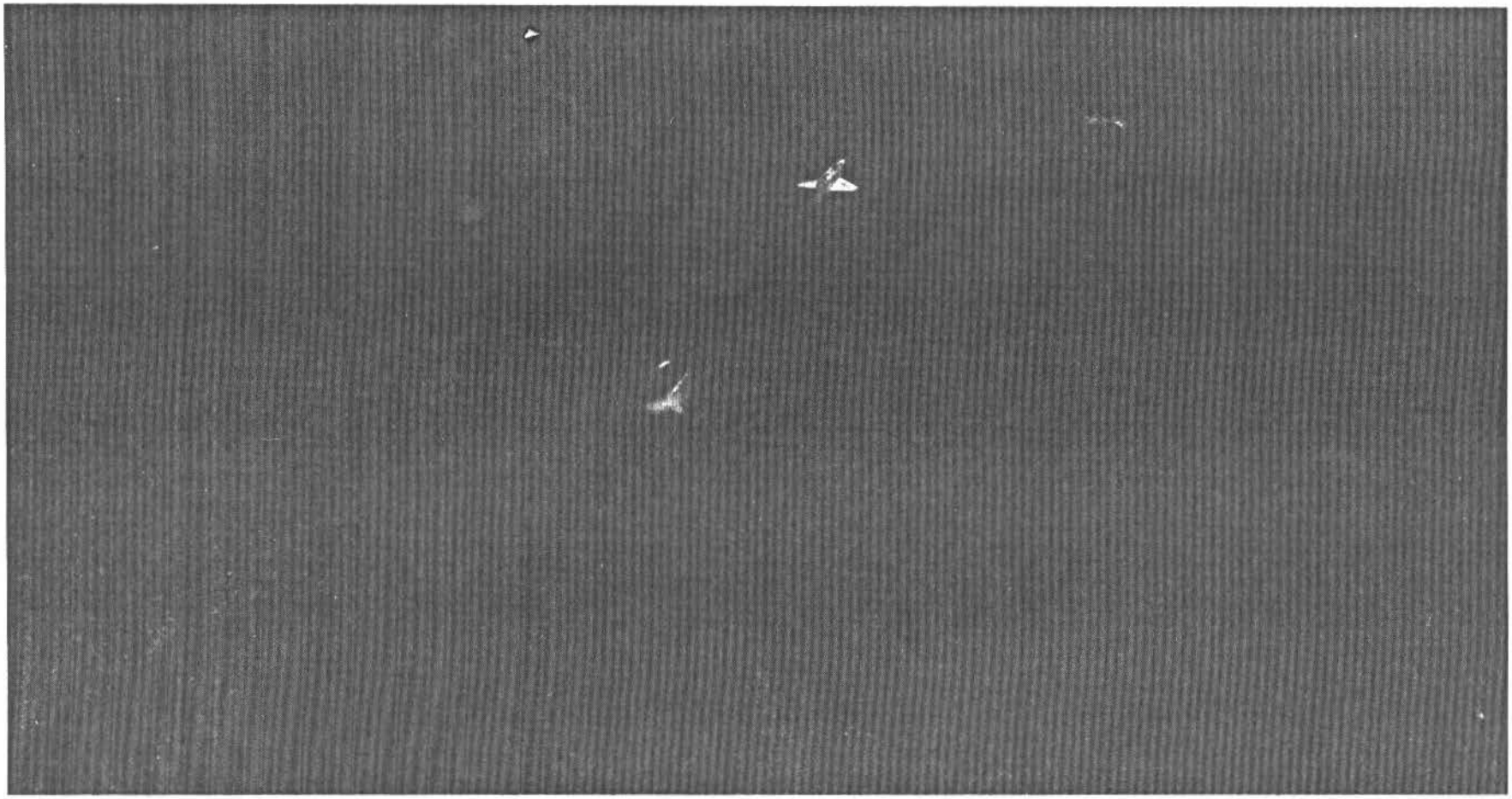

**Figure 1. Infrared Line Scanner Image of a Decks-Awash Submarine off Block Island Recorded in the LWIR Band**

Date: 3 Aug 1970 Time: 1225Q

Only the sail structure of the submarine can be seen distinctly. Note the relative absence of sun glitter.

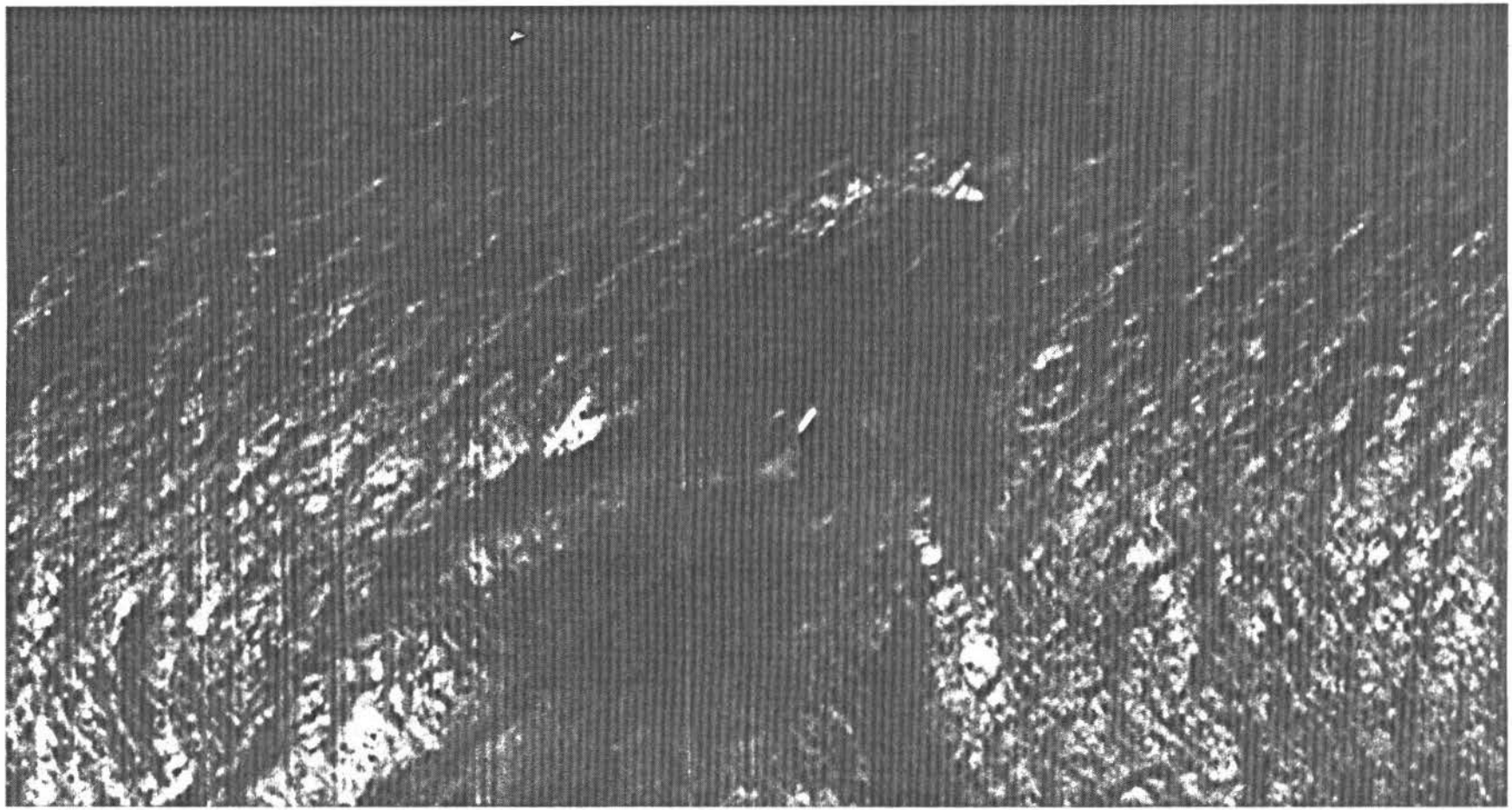

**Figure 2. Infrared Line Scanner Image of a Decks-Awash Submarine off Block Island Recorded in the MWIR Band**

Date: 3 Aug 1970 Time: 1237Q

Note that in this spectral band the sail structure of the submarine is difficult to detect because of sun glitter.

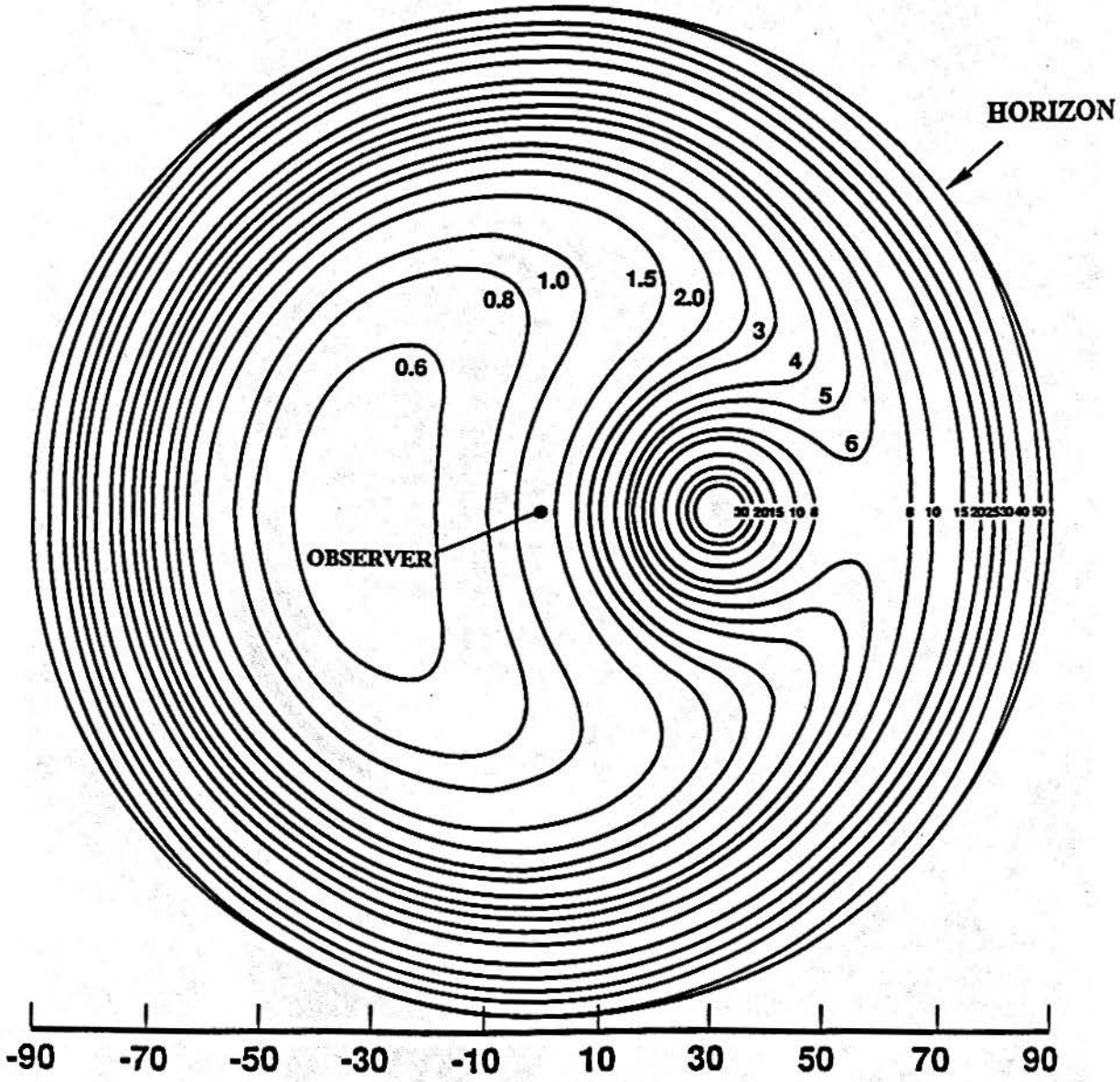


**Figure 3. Calculated Radiance Distribution of a Glitter Pattern from the Sun at a 30° Zenith Angle for a Wavelength of 532 nm as Seen by an Observer Looking Downward at a Breezy Sea Surface.**

Units are $W \cdot m^{-2} \cdot \mu m^{-1} \cdot sr^{-1}$.

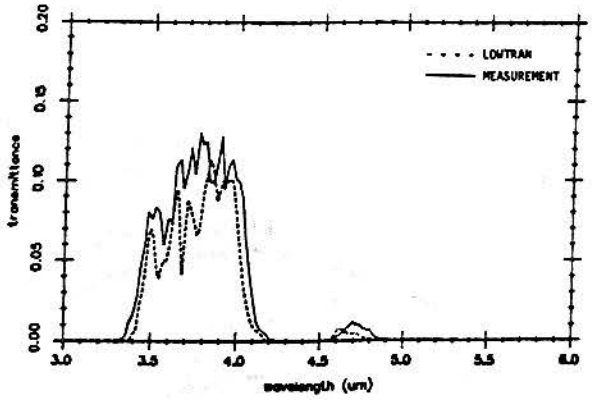


**Figure 4. Measured MWIR Spectral Transmittance over 66.2-km Slant Path vs. LOWTRAN 6 Calculation from Manning et al.[11]**

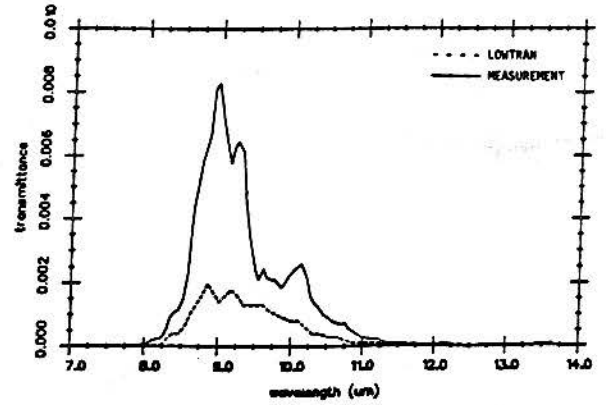


**Figure 5. Measured LWIR Spectral Transmittance over 66.2-km Slant Path vs. LOWTRAN 6 Calculation from Manning et al.[11]**

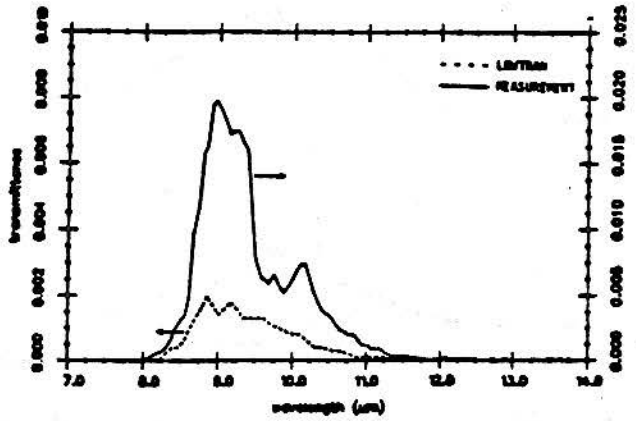

**Figure 6. Measured LWIR Spectral Transmittance over 66.2-km Slant Path vs. LOWTRAN 6 Calculation from Hess et al.[12]**
(The scale for measured values appears on the right.)

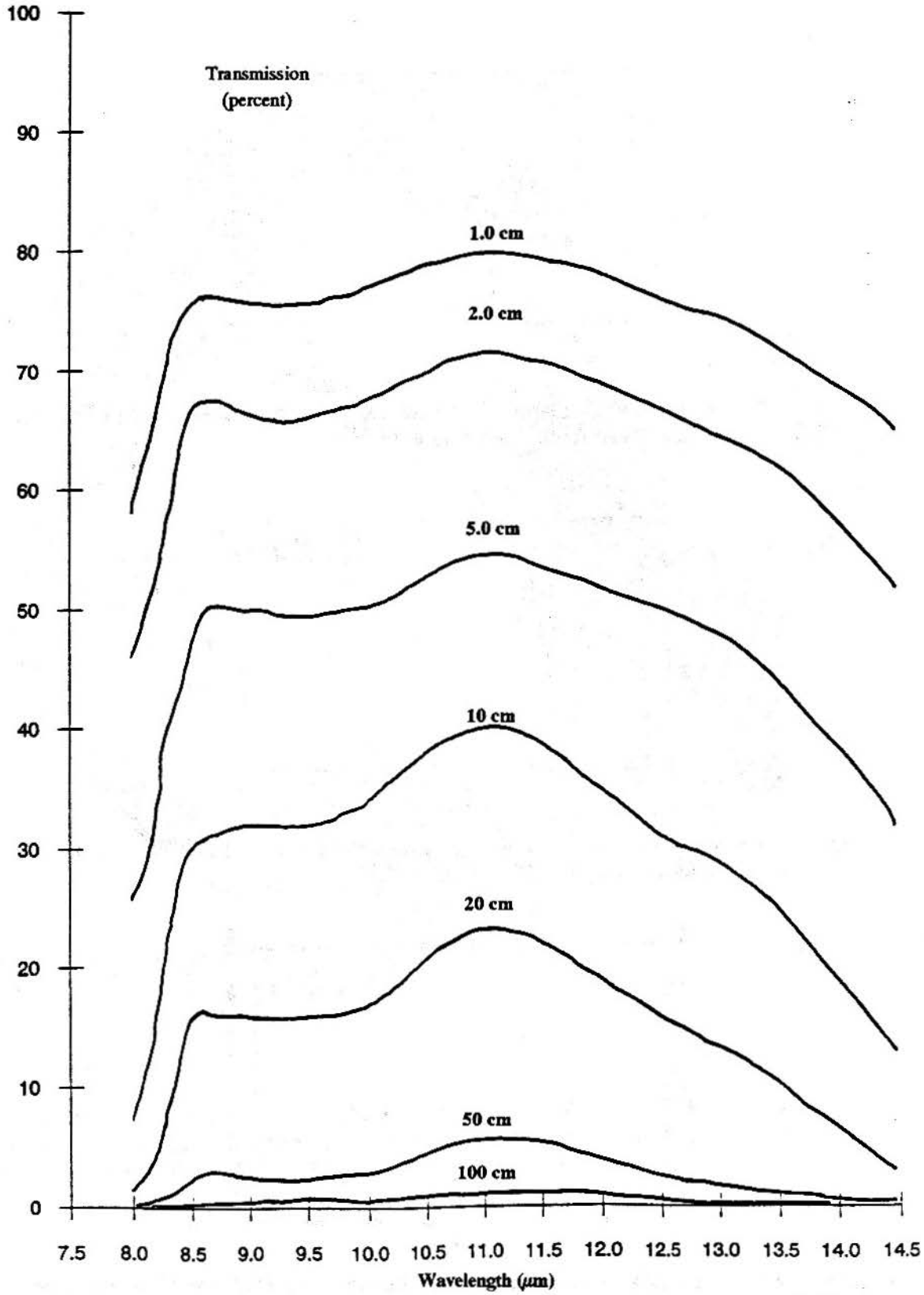


**Figure 7. Percent Spectral Transmission of Infrared Radiation Through Various Amounts of Precipitable Water Vapor at Sea Level, Adapted from Altshuler[13].**

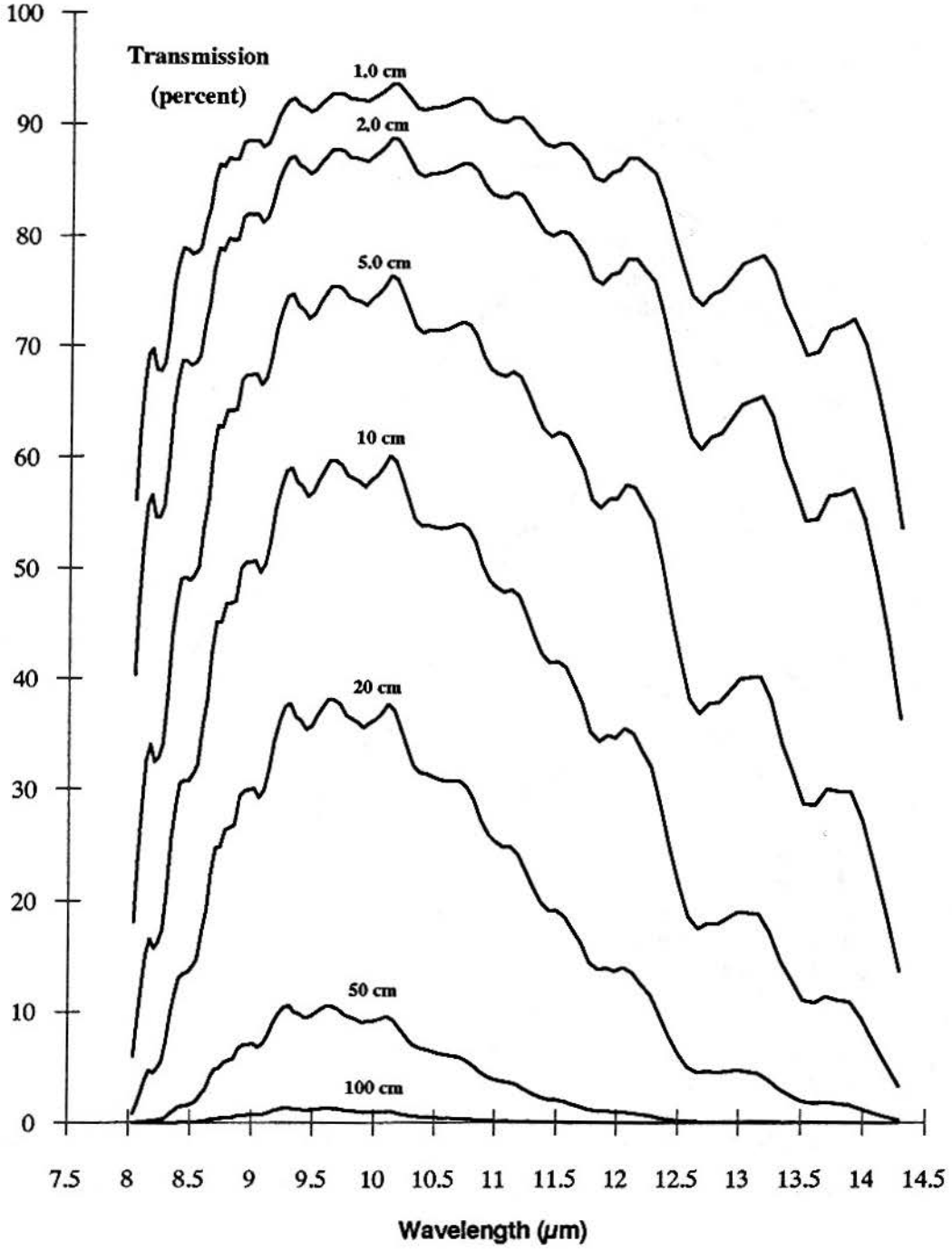


**Figure 8. LOWTRAN 7 Percent Spectral Transmission of Infrared Radiation Through Various Amounts of Precipitable Water Vapor at Sea Level (4.1 g-m$^{-3}$ ).**

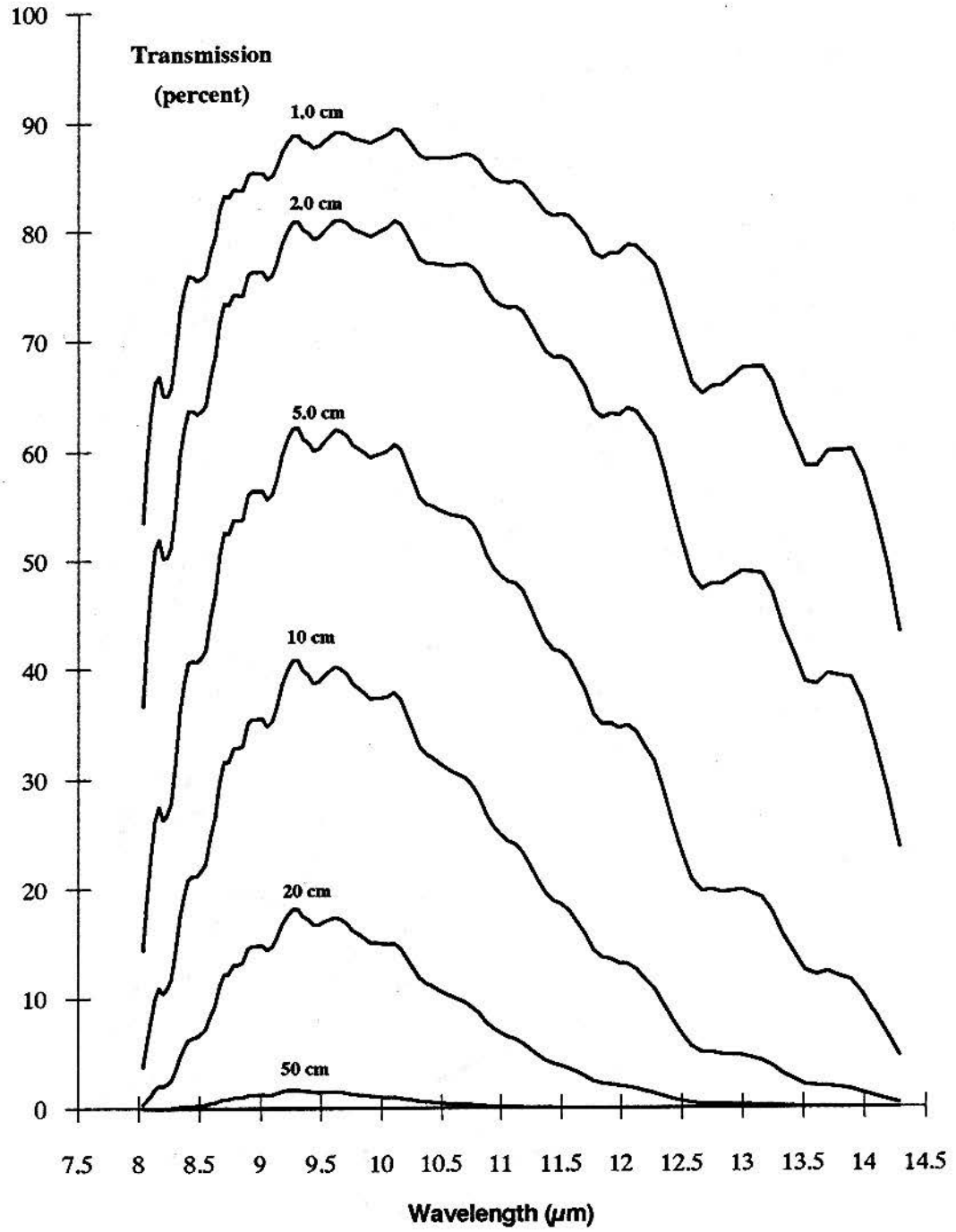


**Figure 9. LOWTRAN 7 Percent Spectral Transmission of Infrared Radiation Through Various Amounts of Precipitable Water Vapor at Sea Level (9.5 g-m$^{-3}$ ).**

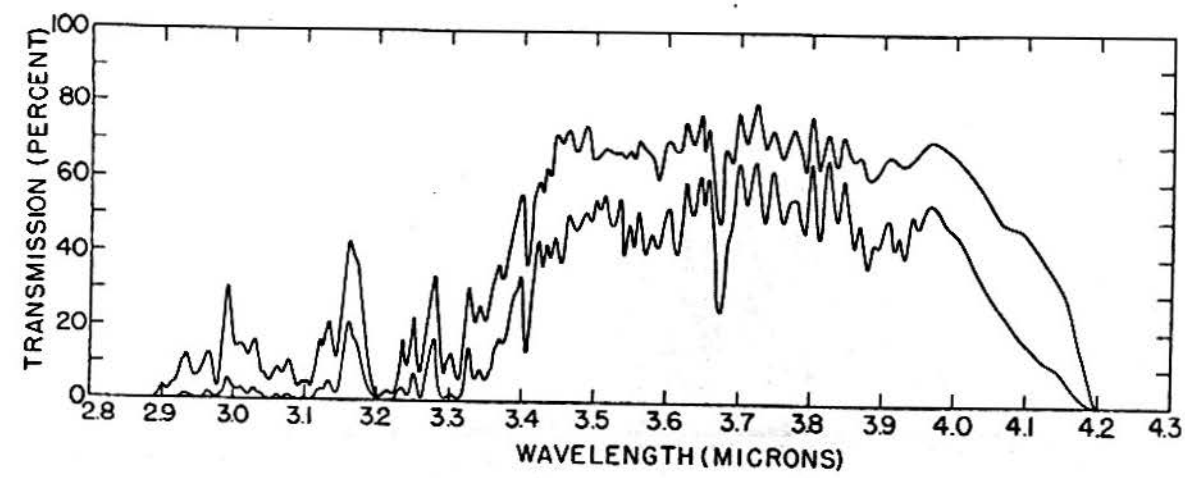


(a)

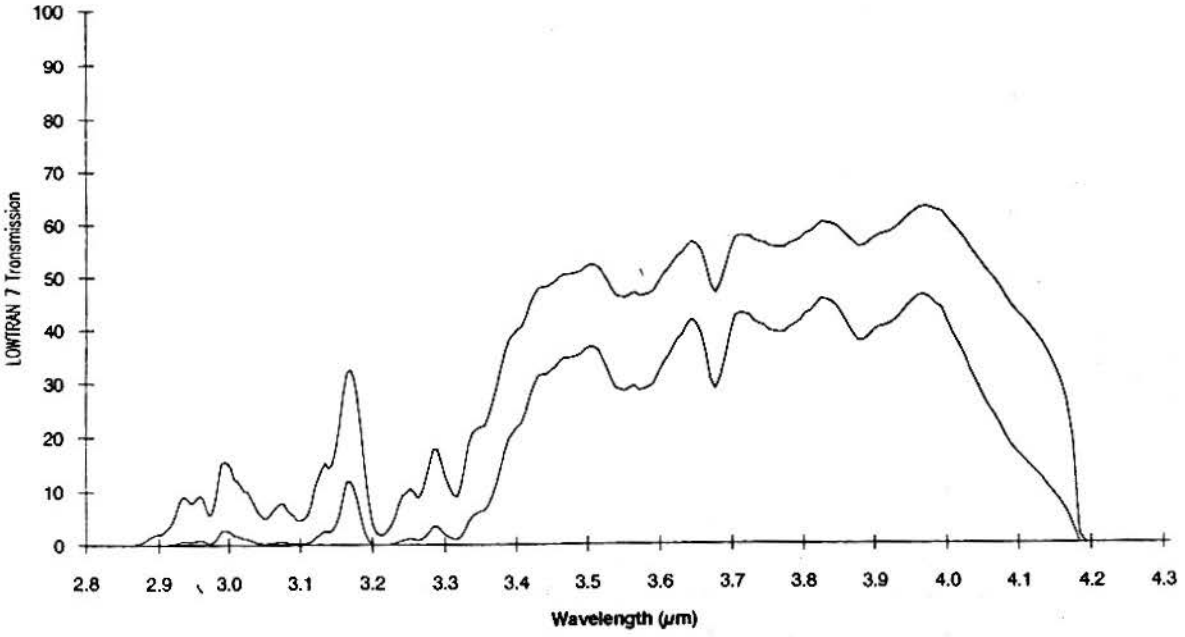


(b)

**Figure 10. Atmospheric Transmission over 5.5 km and 16.25 km paths (2.8-4.3 $\mu$m). (a) Yates and Taylor[9] (b) LOWTRAN 7 Navy Maritime Atmosphere**

5.5 km, 38°F (3.3°C), 66% relative humidity, 2.2 cm $H_2O$ in path, 40% transmission at 0.55 $\mu$m (23.5 km visibility)

16.25 km, 53°F (11.7°C), 41% relative humidity, 6.5-6.9 cm $H_2O$ in path, 29% transmission at 0.55 $\mu$m (51.4 km visibility)

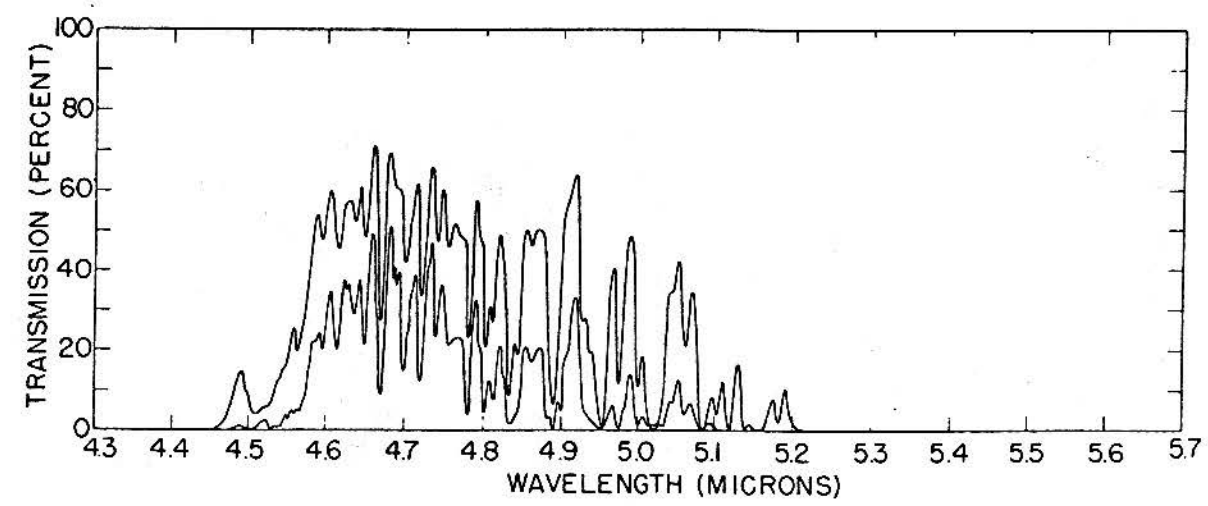


(a)

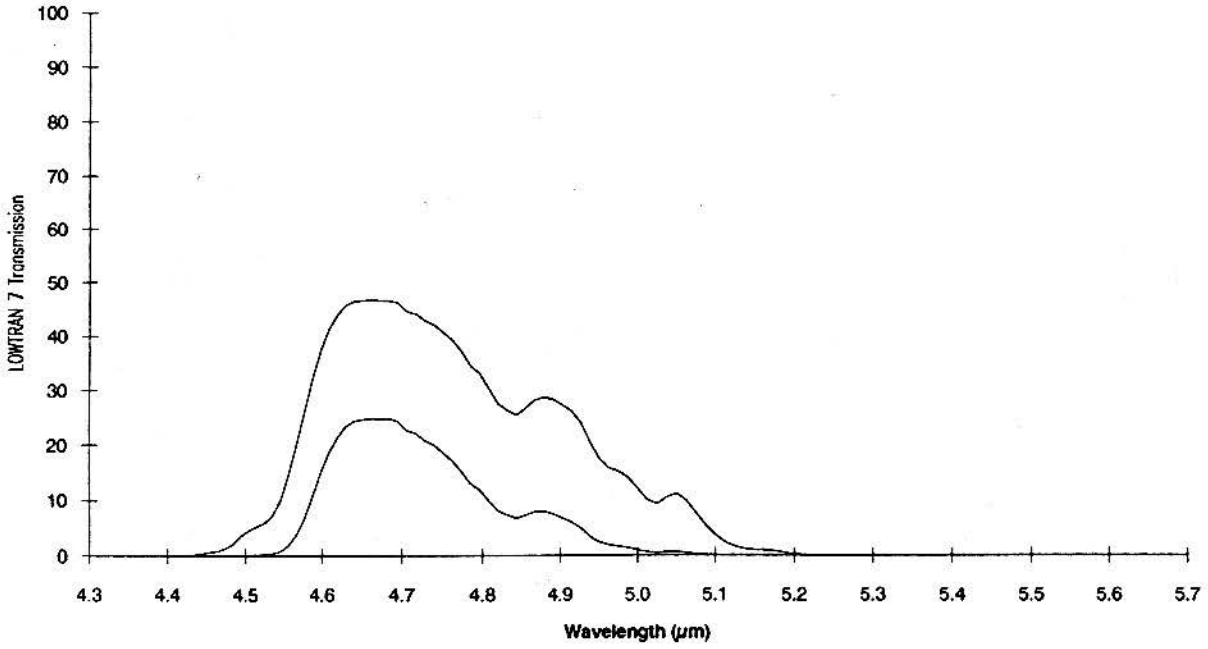


(b)

**Figure 11. Atmospheric Transmission over 5.5 km and 16.25 km paths (4.3-5.7 $\mu$m). (a) Yates and Taylor[9] (b) LOWTRAN 7 Navy Maritime Atmosphere**

5.5 km, 38°F (3.3°C), 66% relative humidity, 2.2 cm $H_2O$ in path, 40% transmission at 0.55 $\mu$m (23.5 km visibility)

16.25 km, 53°F (11.7°C), 41% relative humidity, 6.5-6.9 cm $H_2O$ in path, 29% transmission at 0.55 $\mu$m (51.4 km visibility)

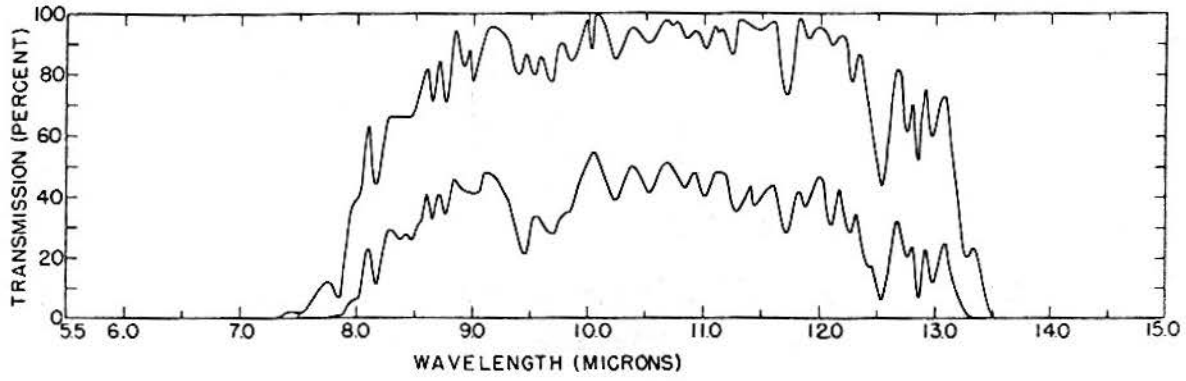


(a)

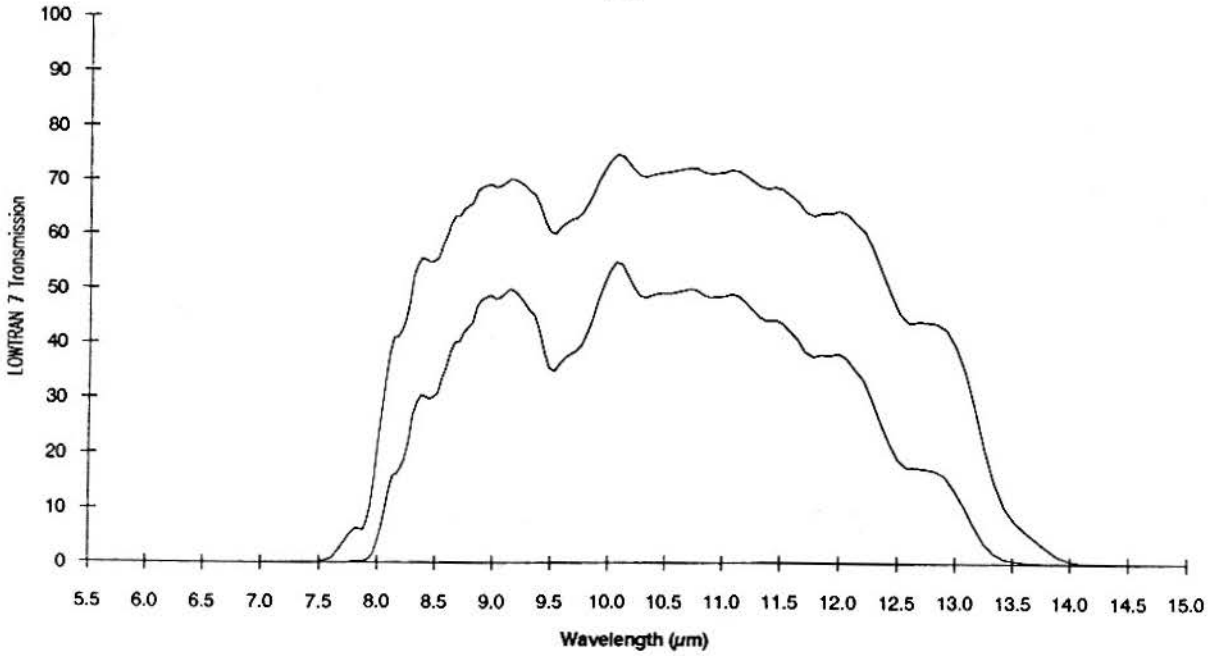


(b)

**Figure 12. Atmospheric Transmission over 5.5 km and 16.25 km paths (5.5-15 $\mu$m). (a) Yates and Taylor[9] (b) LOWTRAN 7 Navy Maritime Atmosphere**

5.5 km, 38°F (3.3°C), 66% relative humidity, 2.2 cm $H_2O$ in path, 40% transmission at 0.55 $\mu$m (23.5 km visibility)

16.25 km, 53°F (11.7°C), 41% relative humidity, 6.5-6.9 cm $H_2O$ in path, 29% transmission at 0.55 $\mu$m (51.4 km visibility)

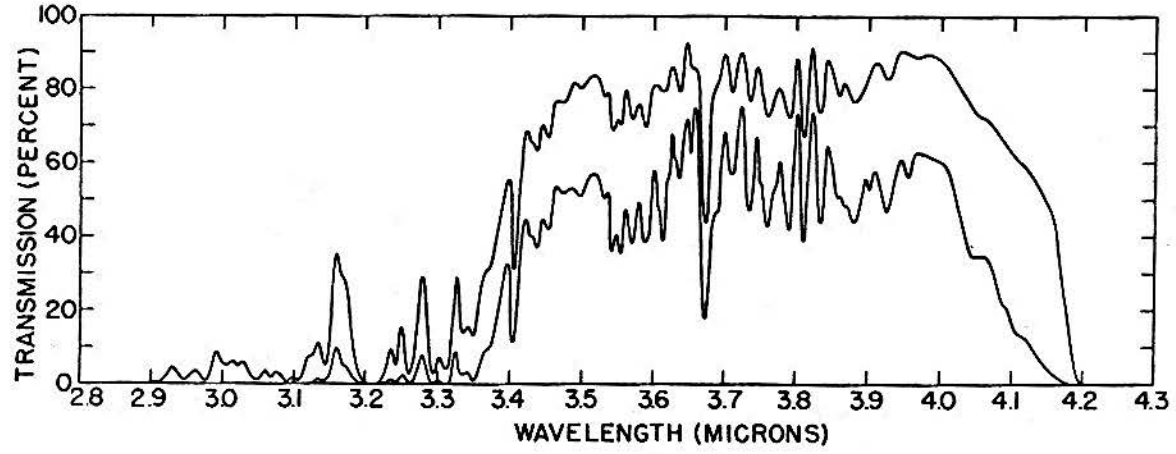


(a)

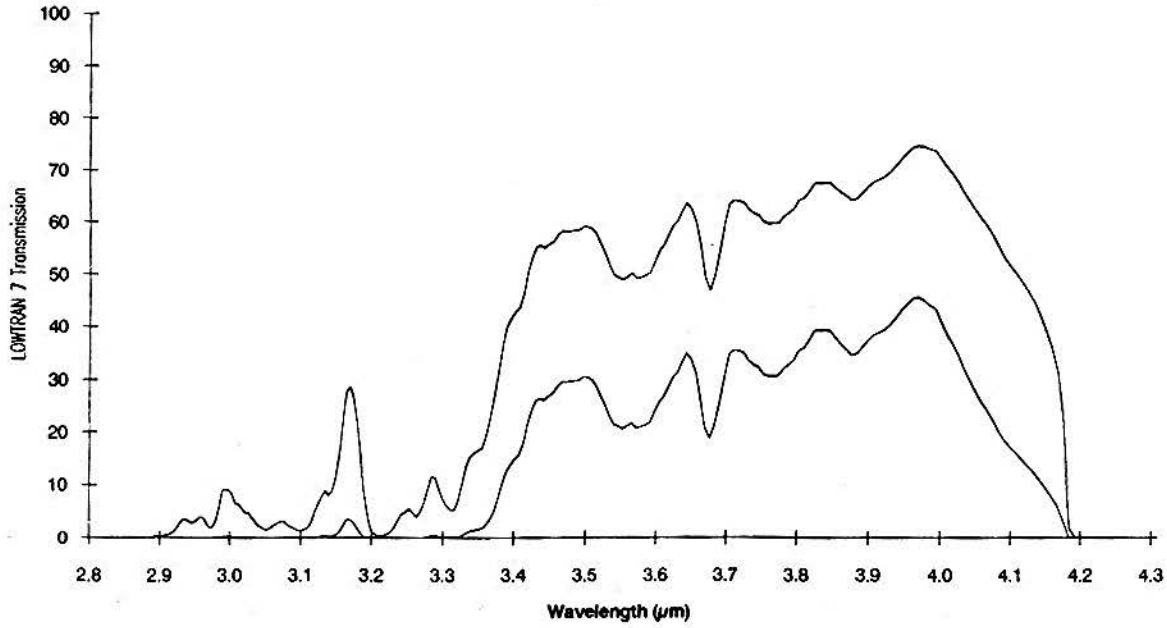


(b)

**Figure 13. Atmospheric Transmission over 5.5 km and 16.25 km paths (2.8-4.3 $\mu$m). (a) Yates and Taylor[9] (b) LOWTRAN 7 Navy Maritime Atmosphere**

5.5 km, 64°F (17.8°C), 51% relative humidity, 4.18 cm $H_2O$ in path, 70% transmission at 0.55 $\mu$m (60.3 km visibility)

16.25 km, 68.7°F (20.4°C), 53% relative humidity, 15.1 cm $H_2O$ in path, 43% transmission at 0.55 $\mu$m (75.3 km visibility)

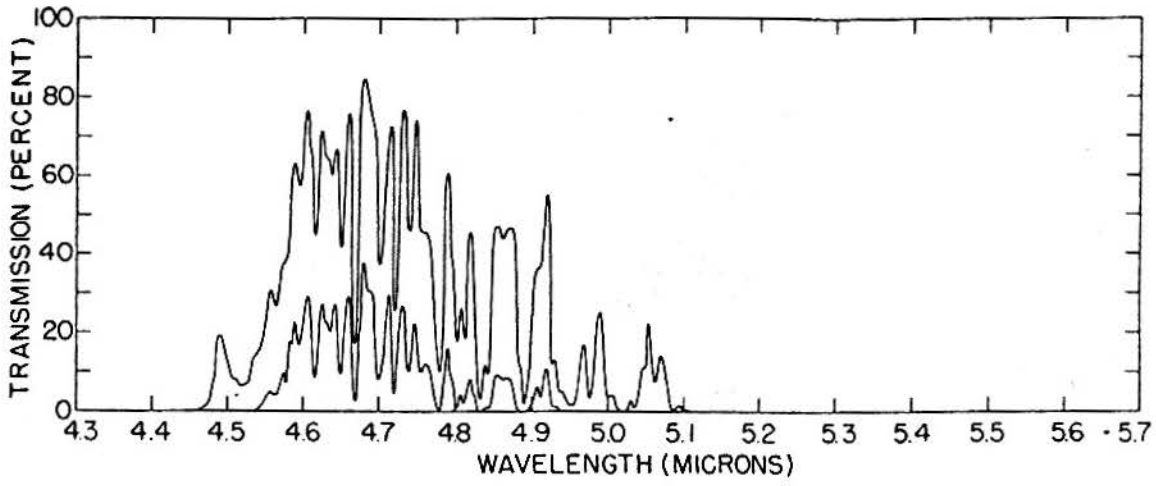


(a)

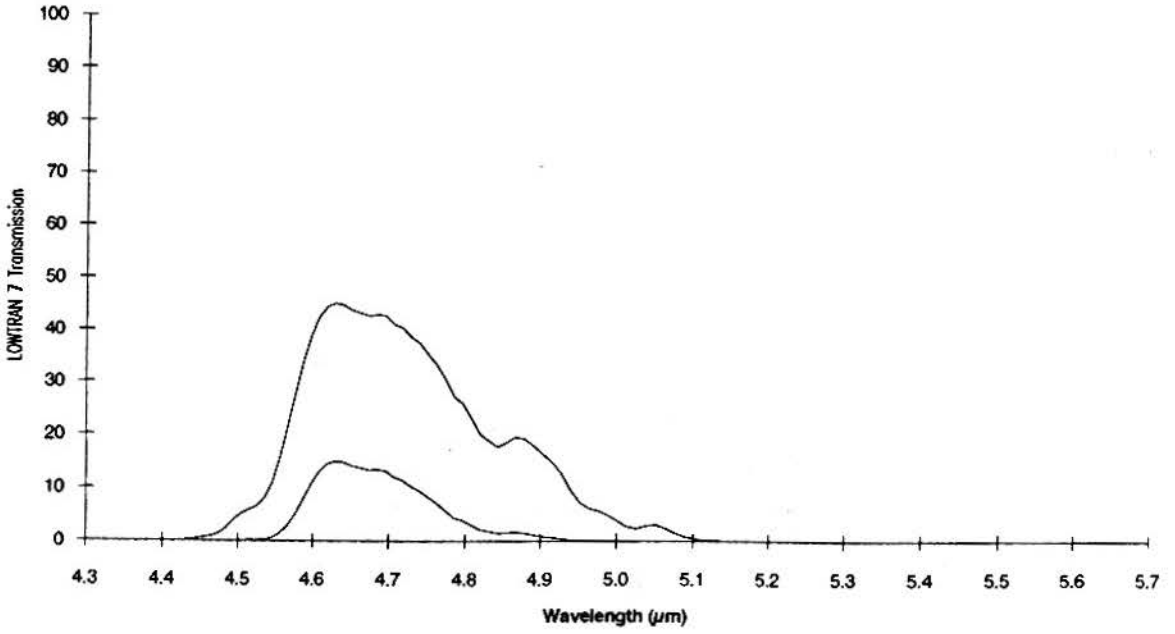


(b)

**Figure 14. Atmospheric Transmission over 5.5 km and 16.25 km paths (4.3-5.7 $\mu$m). (a) Yates and Taylor[9] (b) LOWTRAN 7 Navy Maritime Atmosphere**

5.5 km, 64°F (17.8°C), 51% relative humidity, 4.18 cm $H_2O$ in path, 70% transmission at 0.55 $\mu$m (60.3 km visibility)

16.25 km, 68.7°F (20.4°C), 53% relative humidity, 15.1 cm $H_2O$ in path, 43% transmission at 0.55 $\mu$m (75.3 km visibility)

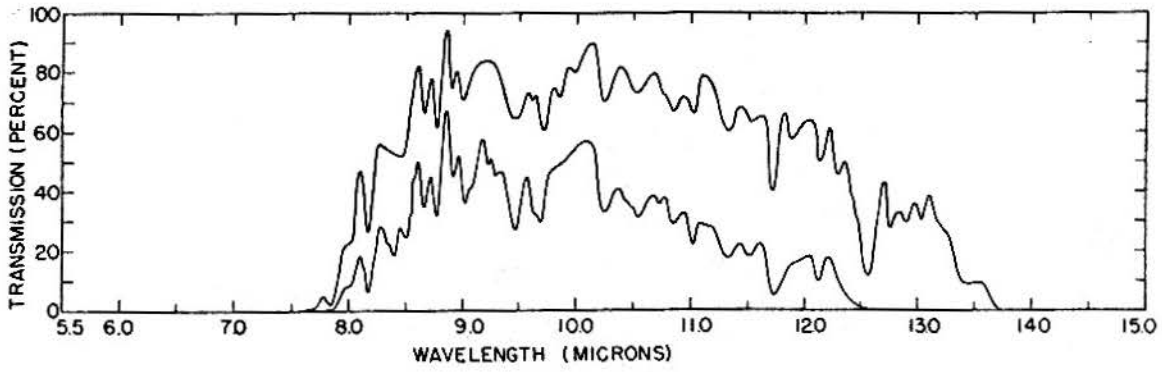


(a)

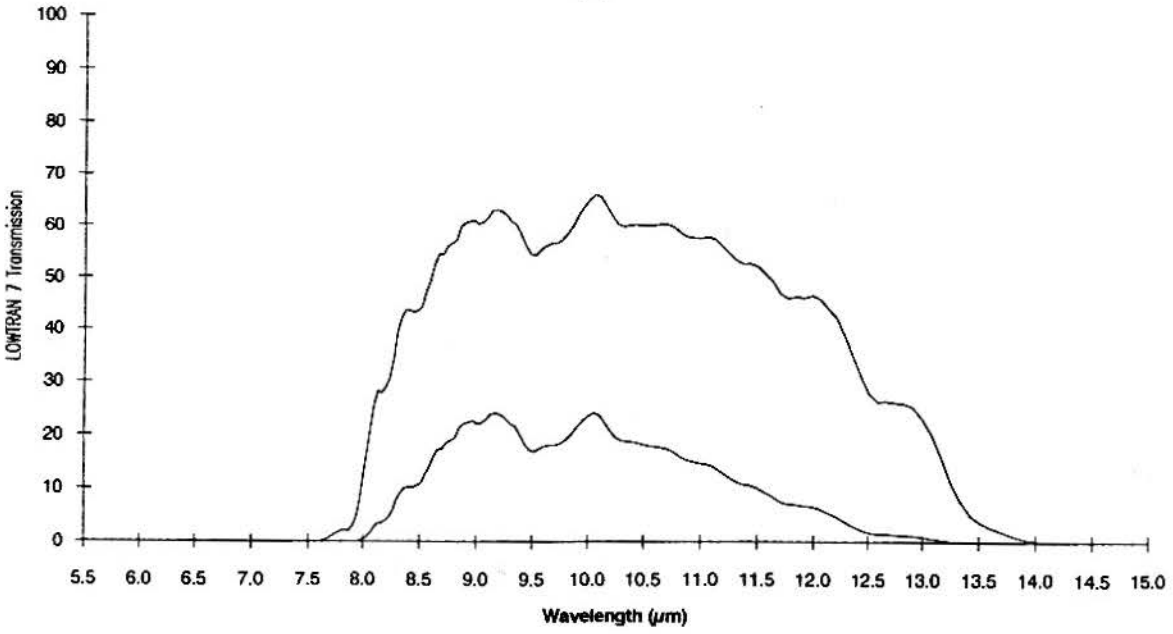


(b)

**Figure 15. Atmospheric Transmission over 5.5 km and 16.25 km paths (5.5-15 $\mu$m). (a) Yates and Taylor[9] (b) LOWTRAN 7 Navy Maritime Atmosphere**

5.5 km, 64°F (17.8°C), 51% relative humidity, 4.18 cm $H_2O$ in path, 70% transmission at 0.55 $\mu$m (60.3 km visibility)

16.25 km, 68.7°F (20.4°C), 53% relative humidity, 15.1 cm $H_2O$ in path, 43% transmission at 0.55 $\mu$m (75.3 km visibility)

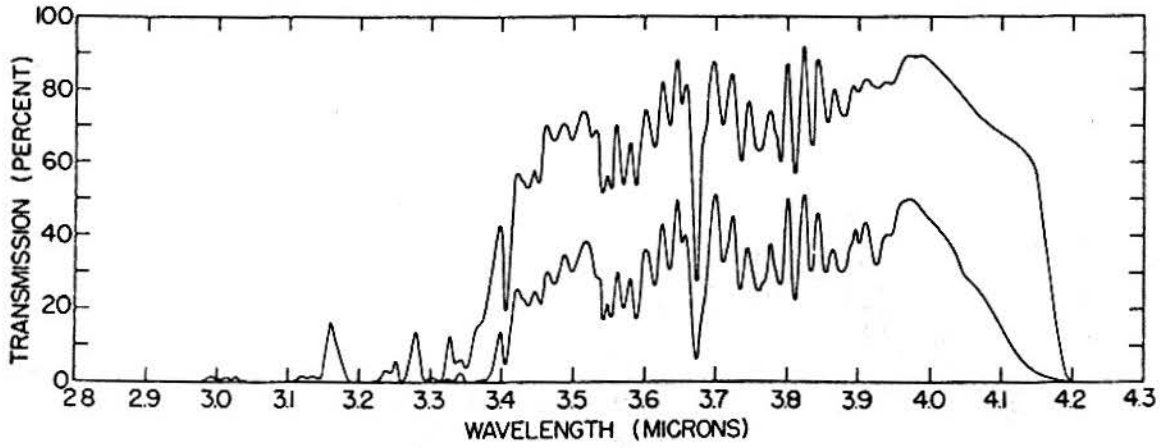


(a)

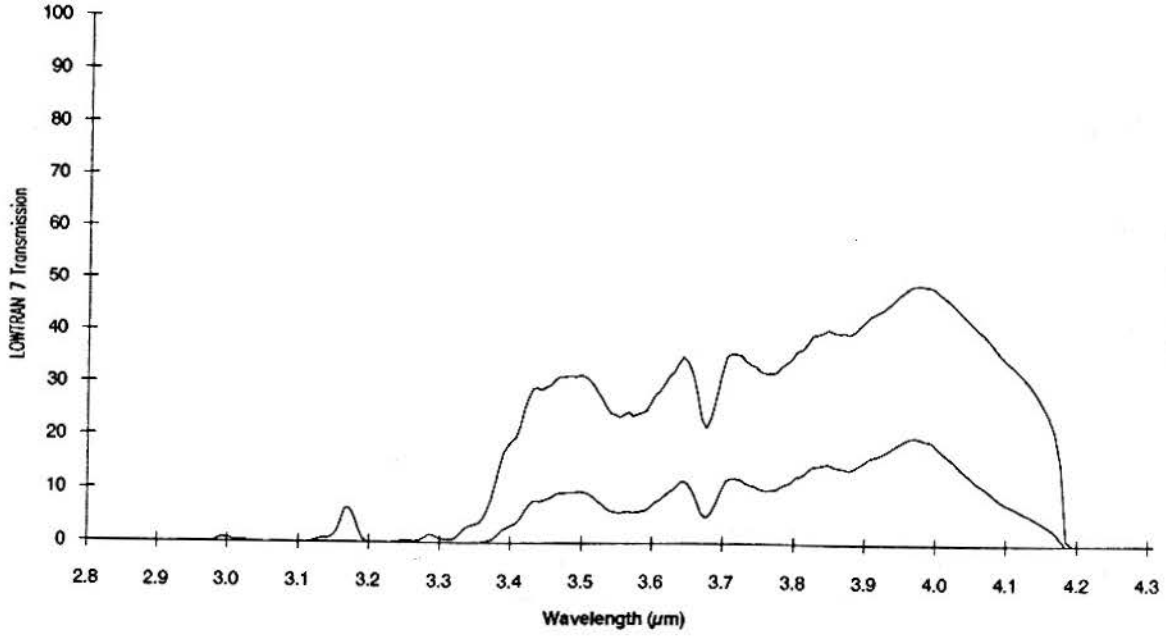


(b)

**Figure 16. Atmospheric Transmission over 5.5 km and 16.25 km paths (2.8-4.3 $\mu$m). (a) Yates and Taylor[9] (b) LOWTRAN 7 Navy Maritime Atmosphere**

5.5 km, 78°F (25.6°C), 73% relative humidity, 9.4 cm $H_2O$ in path, 30% transmission at 0.55 $\mu$m (17.87 km visibility)

16.25 km, 74°F (23.3°C), 82% relative humidity, 27.7 cm $H_2O$ in path, 10% transmission at 0.55 $\mu$m (27.6 km visibility)

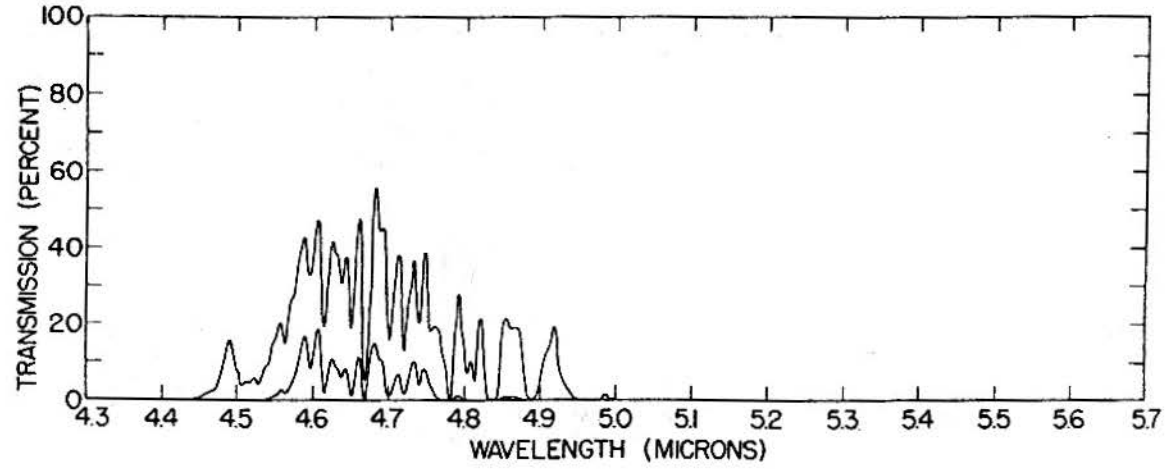


(a)

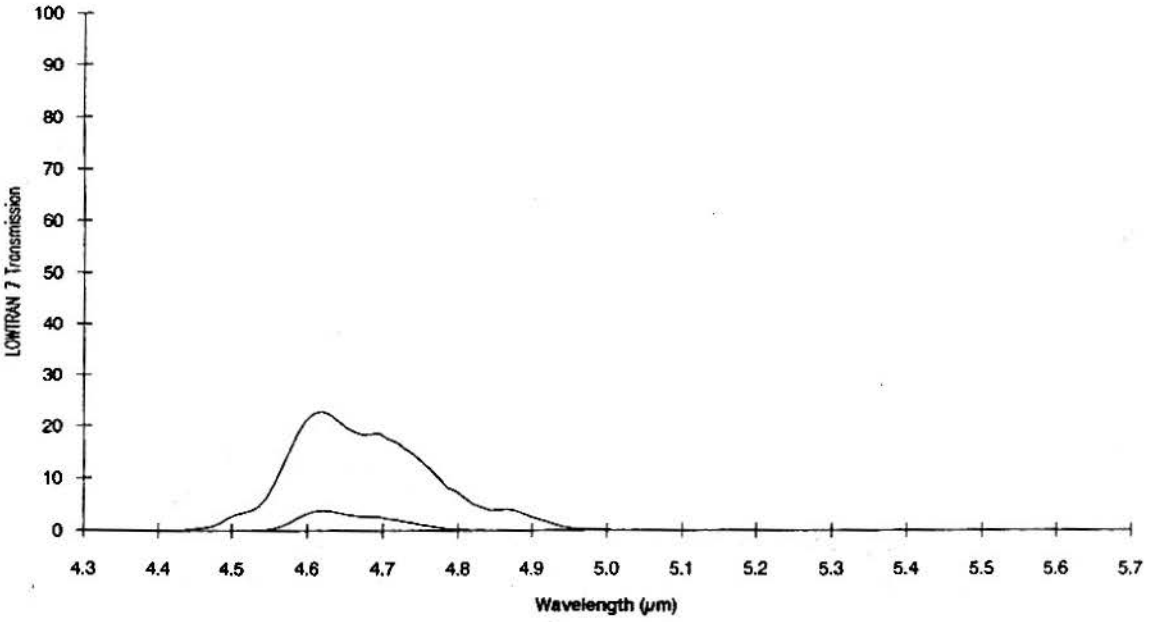


(b)

**Figure 17. Atmospheric Transmission over 5.5 km and 16.25 km paths (4.3-5.7 $\mu$m). (a) Yates and Taylor[9] (b) LOWTRAN 7 Navy Maritime Atmosphere**

5.5 km, 78°F (25.6°C), 73% relative humidity, 9.4 cm $H_2O$ in path, 30% transmission at 0.55 $\mu$m (17.87 km visibility)

16.25 km, 74°F (23.3°C), 82% relative humidity, 27.7 cm $H_2O$ in path, 10% transmission at 0.55 $\mu$m (27.6 km visibility)

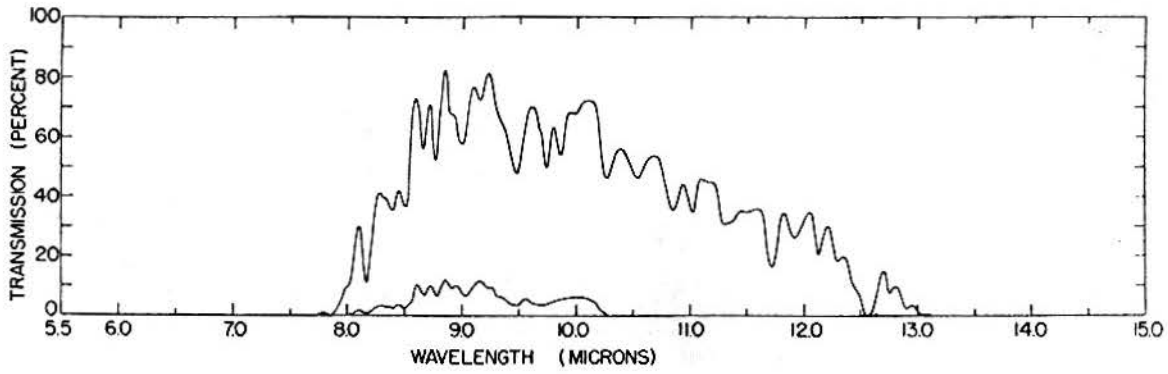


(a)

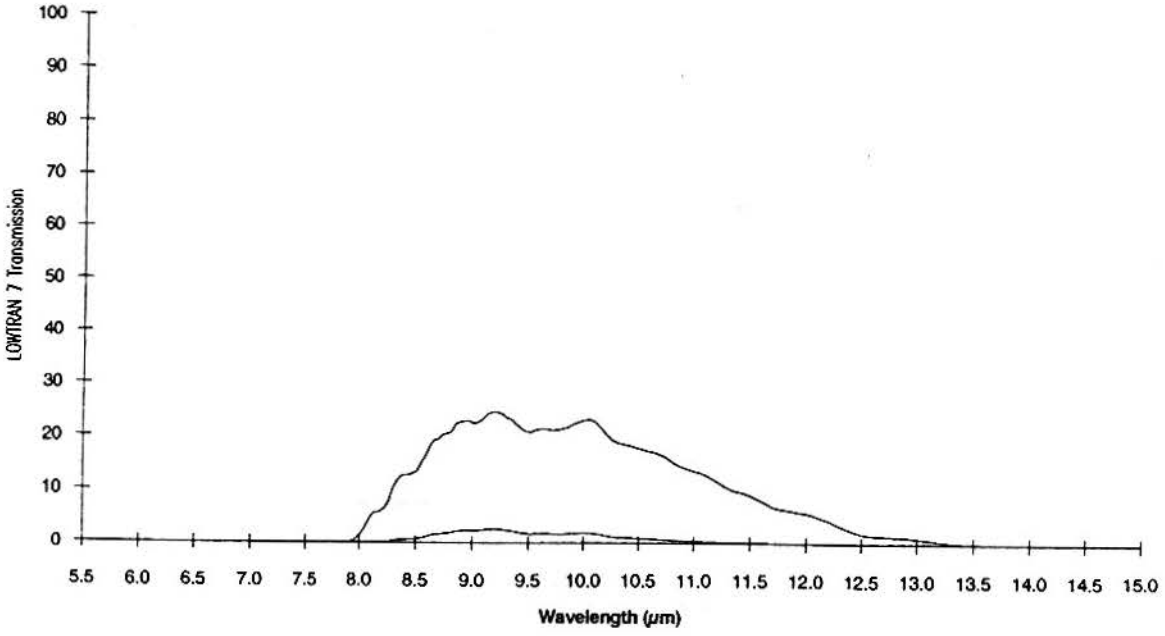


(b)

**Figure 18. Atmospheric Transmission over 5.5 km and 16.25 km paths (5.5-15 $\mu$m). (a) Yates and Taylor[9] (b) LOWTRAN 7 Navy Maritime Atmosphere**

5.5 km, 78°F (25.6°C), 73% relative humidity, 9.4 cm $H_2O$ in path, 30% transmission at 0.55 $\mu$m (17.9 km visibility)

16.25 km, 74°F (23.3°C), 82% relative humidity, 27.7 cm $H_2O$ in path, 10% transmission at 0.55 $\mu$m (27.6 km visibility)

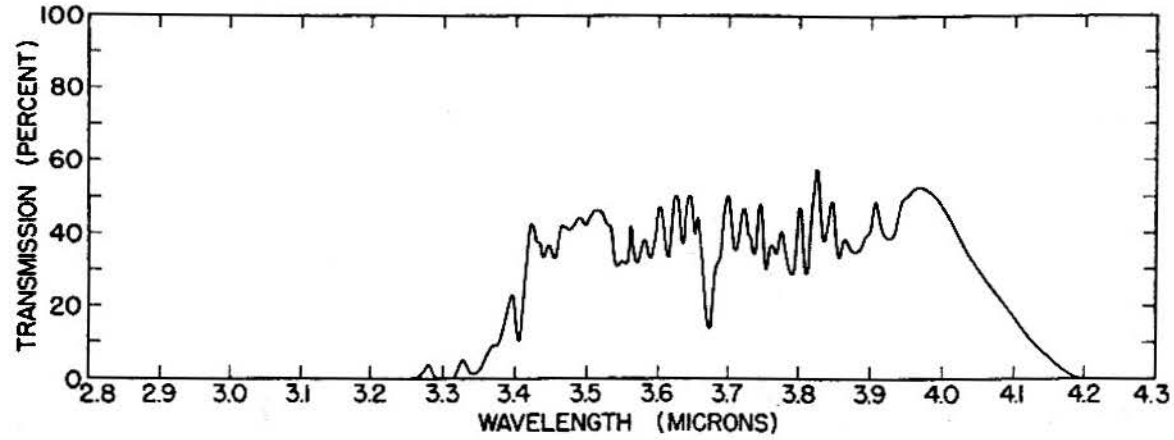


(a)

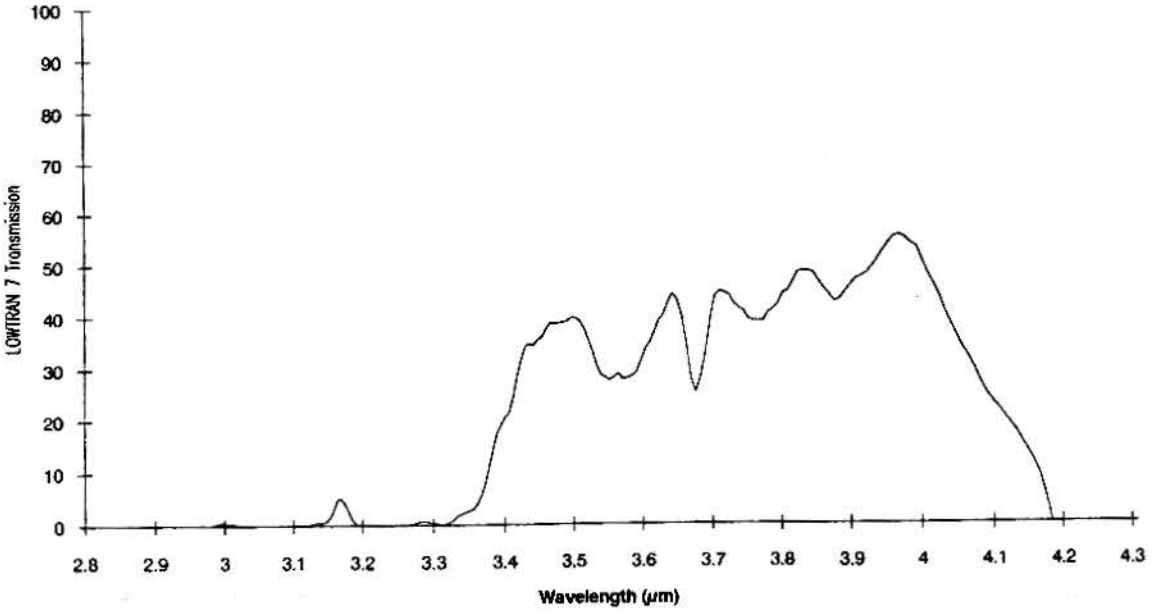


(b)

**Figure 19. Atmospheric Transmission over 27.7 km path (2.8-4.3 $\mu$m). (a) Yates and Taylor[9] (b) LOWTRAN 7 Navy Maritime Atmosphere**

27.7 km, 10,000 ft average altitude, 43°F (6.1°C), 100% relative humidity, 20 cm $H_2O$ in path, 26.5% transmission at 0.55 $\mu$m (81.6 km visibility)

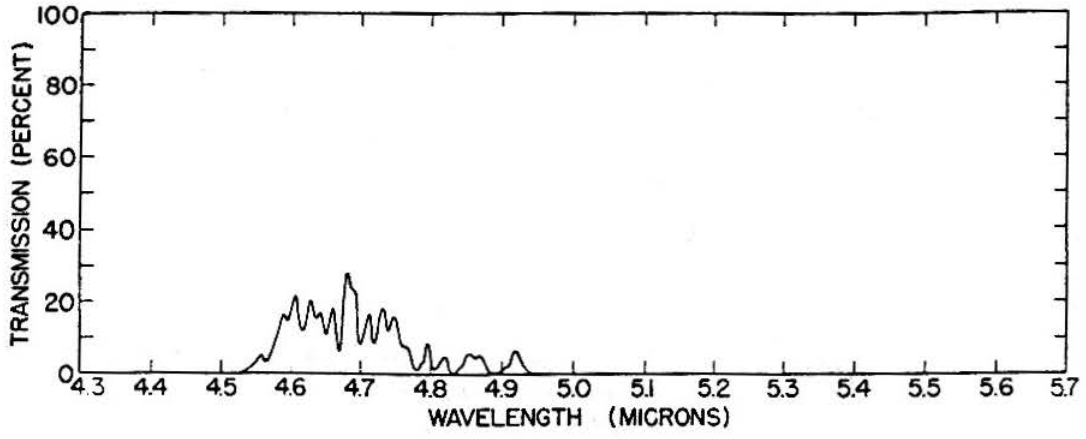


(a)

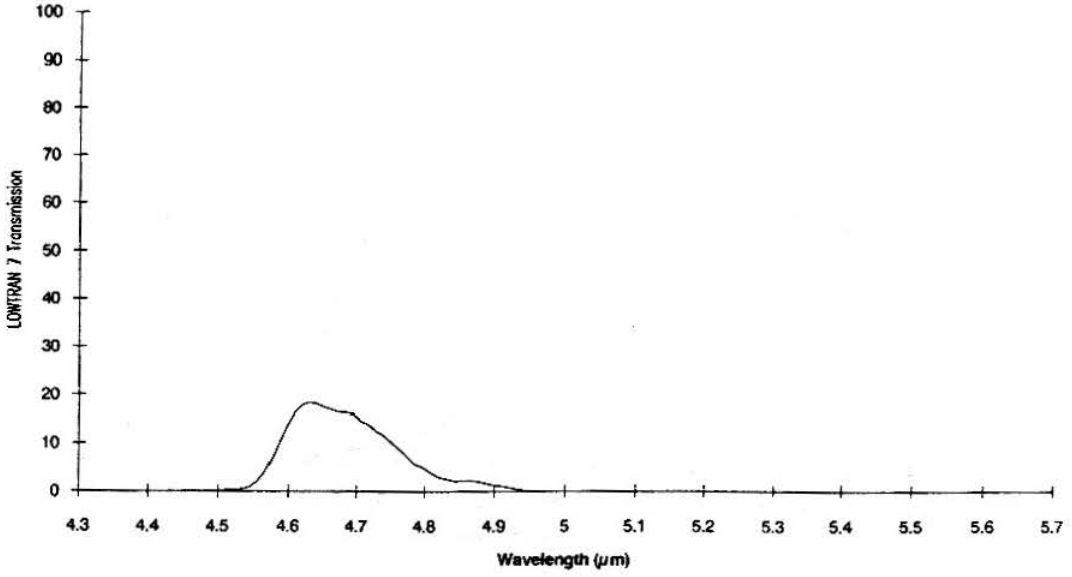


(b)

**Figure 20. Atmospheric Transmission over 27.7 km path (4.3-5.7 $\mu$m). (a) Yates and Taylor[9] (b) LOWTRAN 7 Navy Maritime Atmosphere**

27.7 km, 10,000 ft average altitude, 43°F (6.1°C), 100% relative humidity, 20 cm $H_2O$ in path, 26.5% transmission at 0.55 $\mu$m (81.6 km visibility)

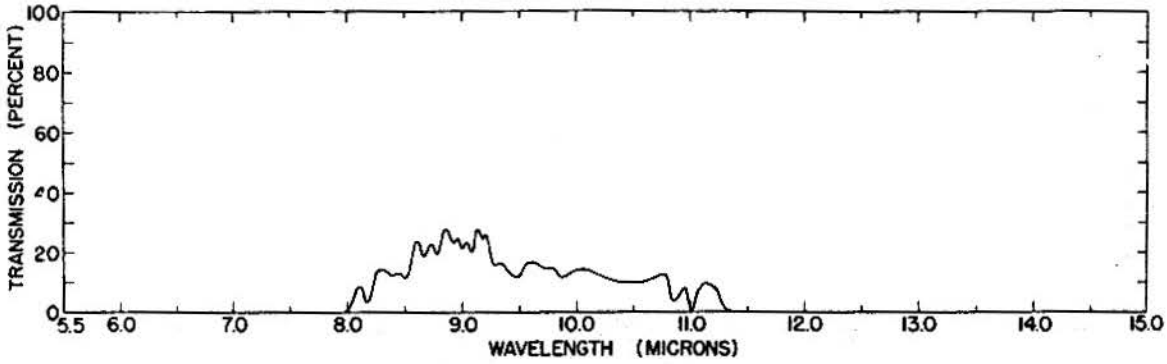


(a)

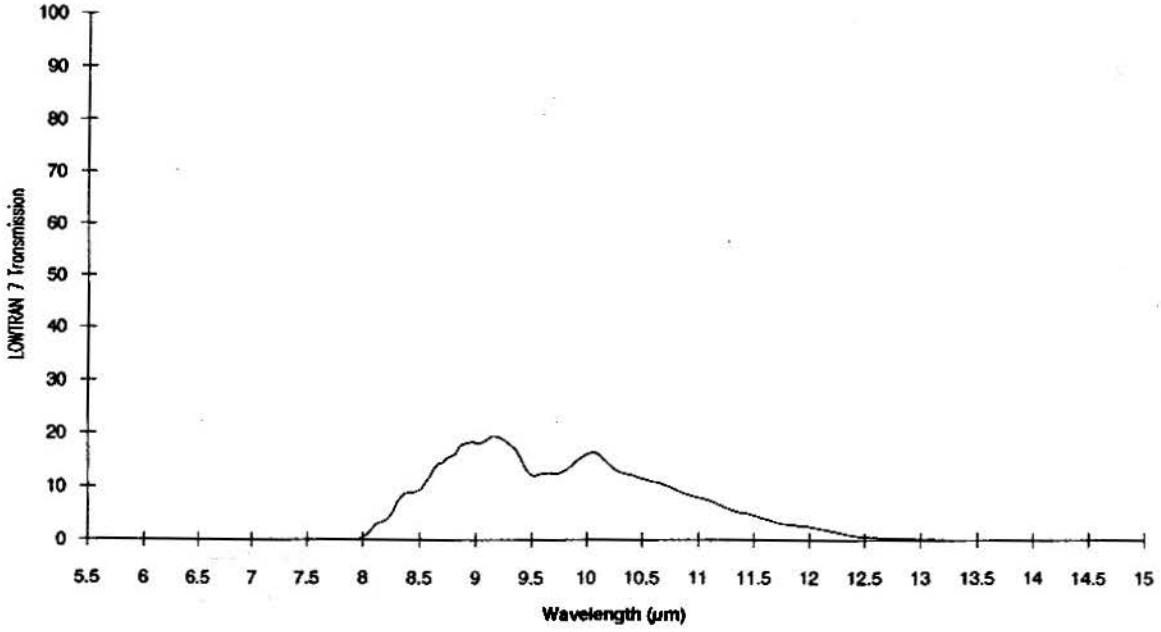


(b)

**Figure 21. Atmospheric Transmission over 27.7 km path (5.5-15 $\mu$m). (a) Yates and Taylor[9] (b) LOWTRAN 7 Navy Maritime Atmosphere**

27.7 km, 10,000 ft average altitude, 43°F (6.1°C), 100% relative humidity, 20 cm $H_2O$ in path, 26.5% transmission at 0.55 $\mu$m (81.6 km visibility)

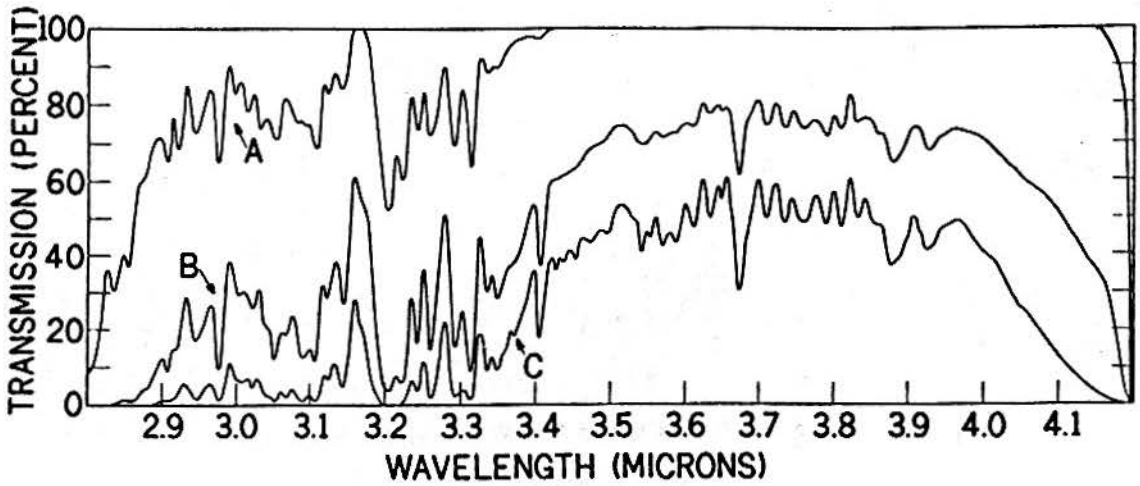


(a)

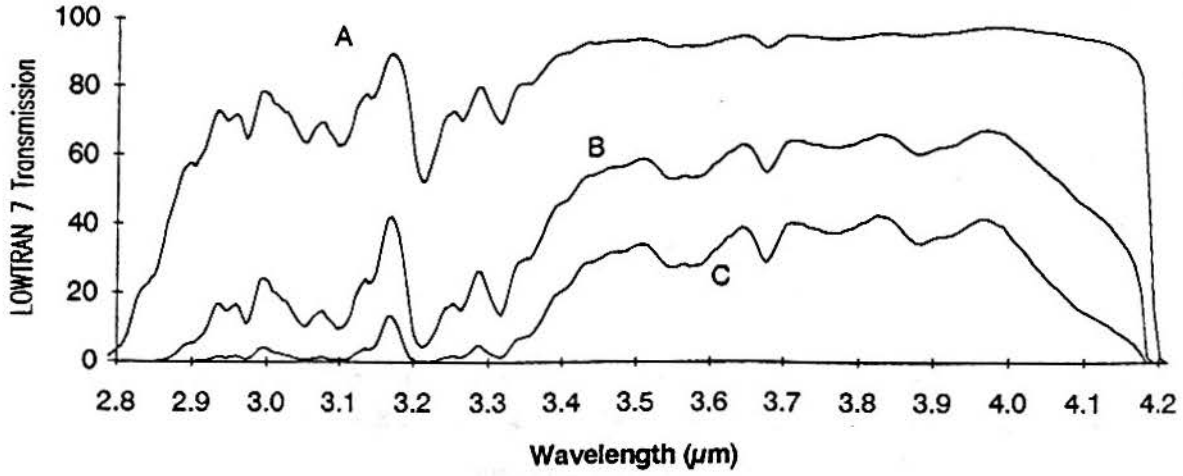


(b)

**Figure 22. Atmospheric Transmission over 0.3, 5.5, and 16.25 km paths (2.8-4.2 μm). (a) Yates and Taylor[7] (b) LOWTRAN 7 Navy Maritime Atmosphere**

Curve A, 0.305 km, 37°F (2.8°C), 62% relative humidity, 0.11 cm $H_2O$ in path, 35.4 km visibility

Curve B, 5.5 km, 34.5°F (1.4°C), 47% relative humidity, 1.37 cm $H_2O$ in path, 25.8 km visibility

Curve C, 16.25 km, 40.5°F (4.7°C), 48% relative humidity, 5.2 cm $H_2O$ in path, 38.6 km visibility

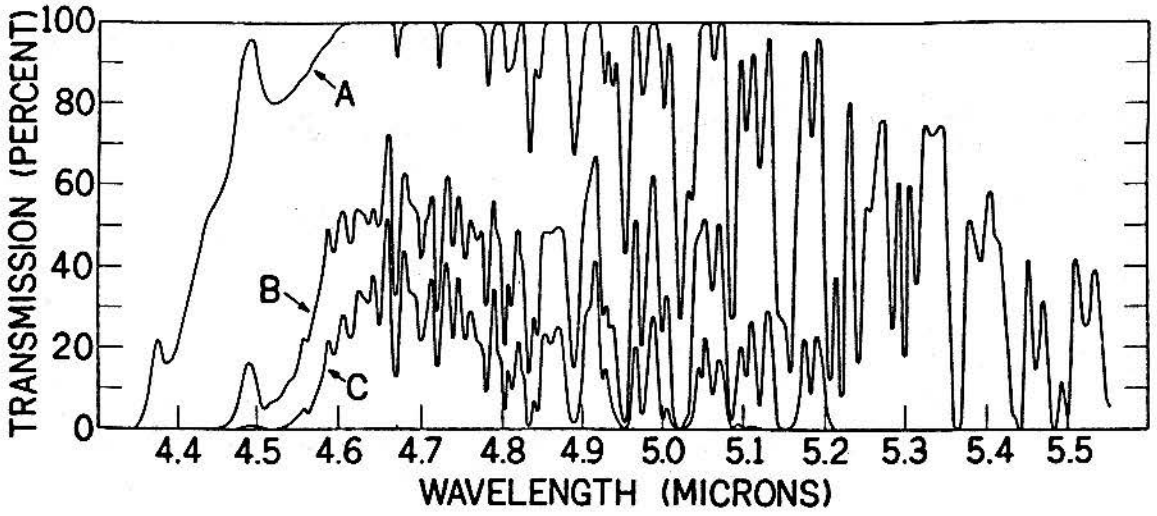


(a)

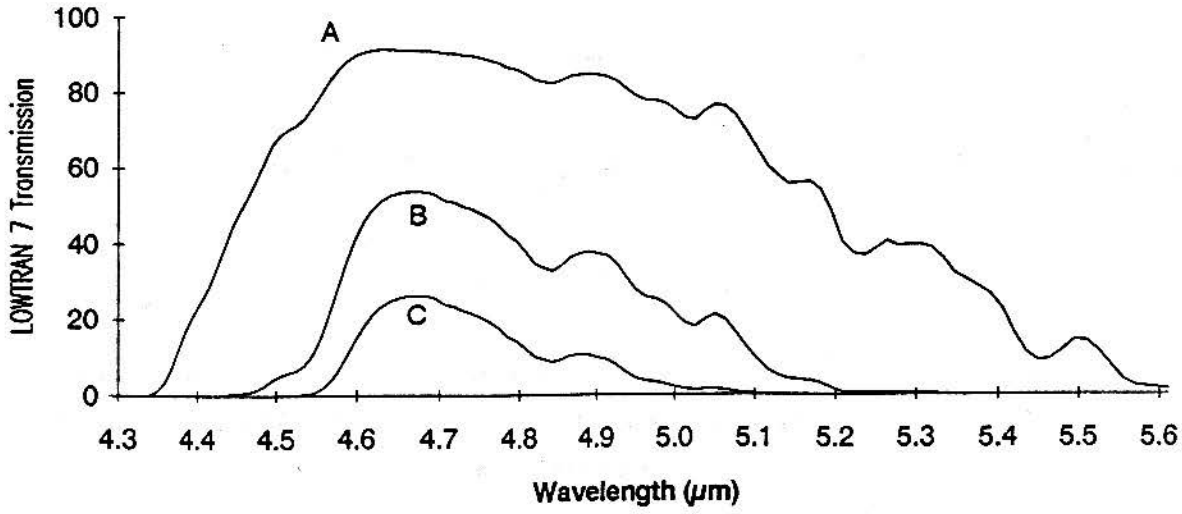


(b)

**Figure 23. Atmospheric Transmission over 0.3, 5.5, and 16.25 km paths (4.3-5.6 μm). (a) Yates and Taylor[7] (b) LOWTRAN 7 Navy Maritime Atmosphere**

Curve A, 0.305 km, 37°F (2.8°C), 62% relative humidity, 0.11 cm $H_2O$ in path, 35.4 km visibility

Curve B, 5.5 km, 34.5°F (1.4°C), 47% relative humidity, 1.37 cm $H_2O$ in path, 25.8 km visibility

Curve C, 16.25 km, 40.5°F (4.7°C), 48% relative humidity, 5.2 cm $H_2O$ in path, 38.6 km visibility

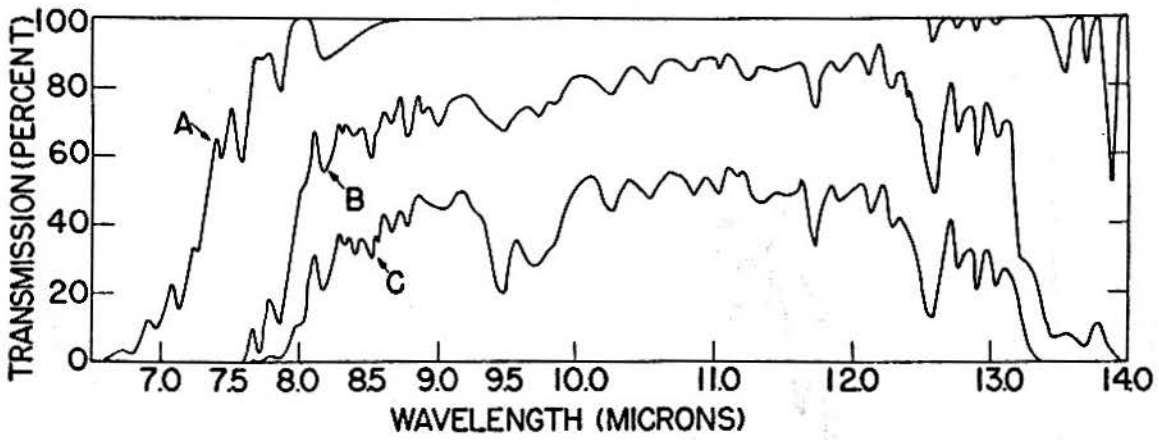


(a)

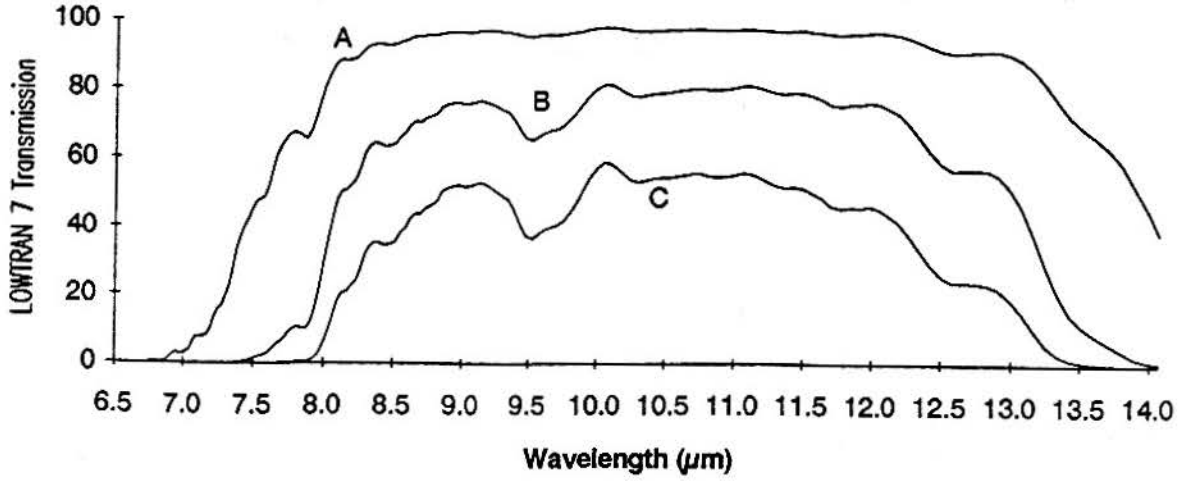


(b)

**Figure 24. Atmospheric Transmission over 0.3, 5.5, and 16.25 km paths (6.5-14 μm). (a) Yates and Taylor[7] (b) LOWTRAN 7 Navy Maritime Atmosphere**

Curve A, 0.305 km, 37°F (2.8°C), 62% relative humidity, 0.11 cm $H_2O$ in path, 35.4 km visibility

Curve B, 5.5 km, 34.5°F (1.4°C), 47% relative humidity, 1.37 cm $H_2O$ in path, 25.8 km visibility

Curve C, 16.25 km, 40.5°F (4.7°C), 48% relative humidity, 5.2 cm $H_2O$ in path, 38.6 km visibility

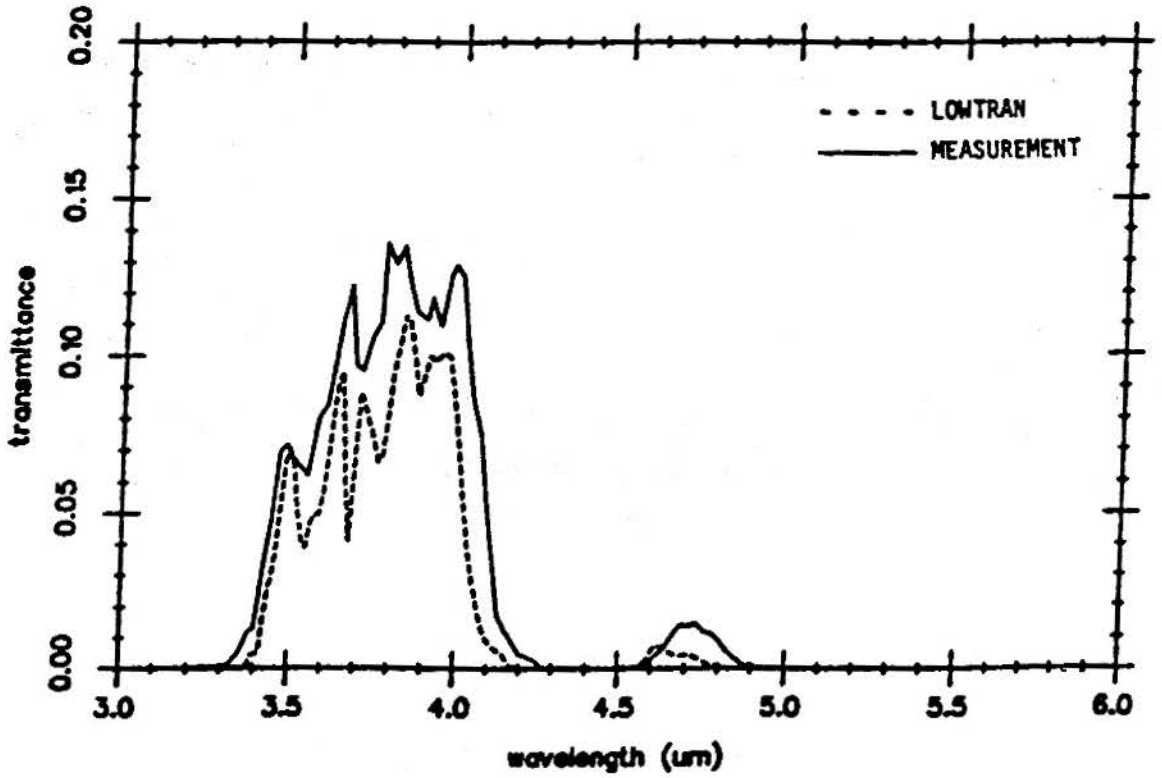


(a)

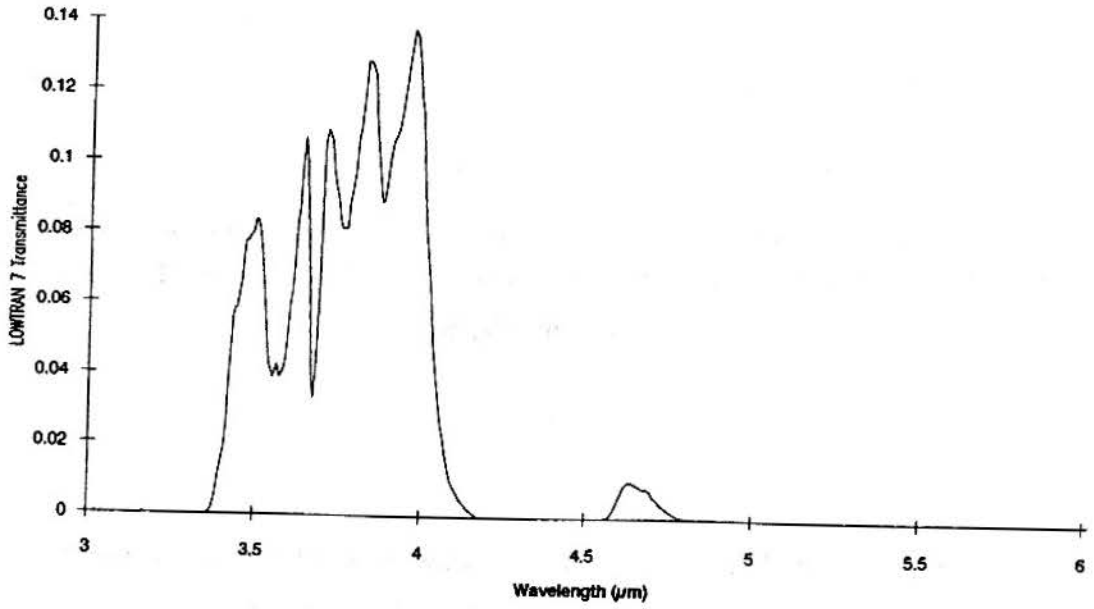


(b)

**Figure 25. Atmospheric Transmission over 66.2 km Path with the Radiosonde Profiles of Figure 27 (3-6 $\mu$m).**

**(a) Measured and LOWTRAN 6 curves from Manning et al[11]**

**(b) LOWTRAN 7 Navy Maritime Atmosphere 100 km Visibility**

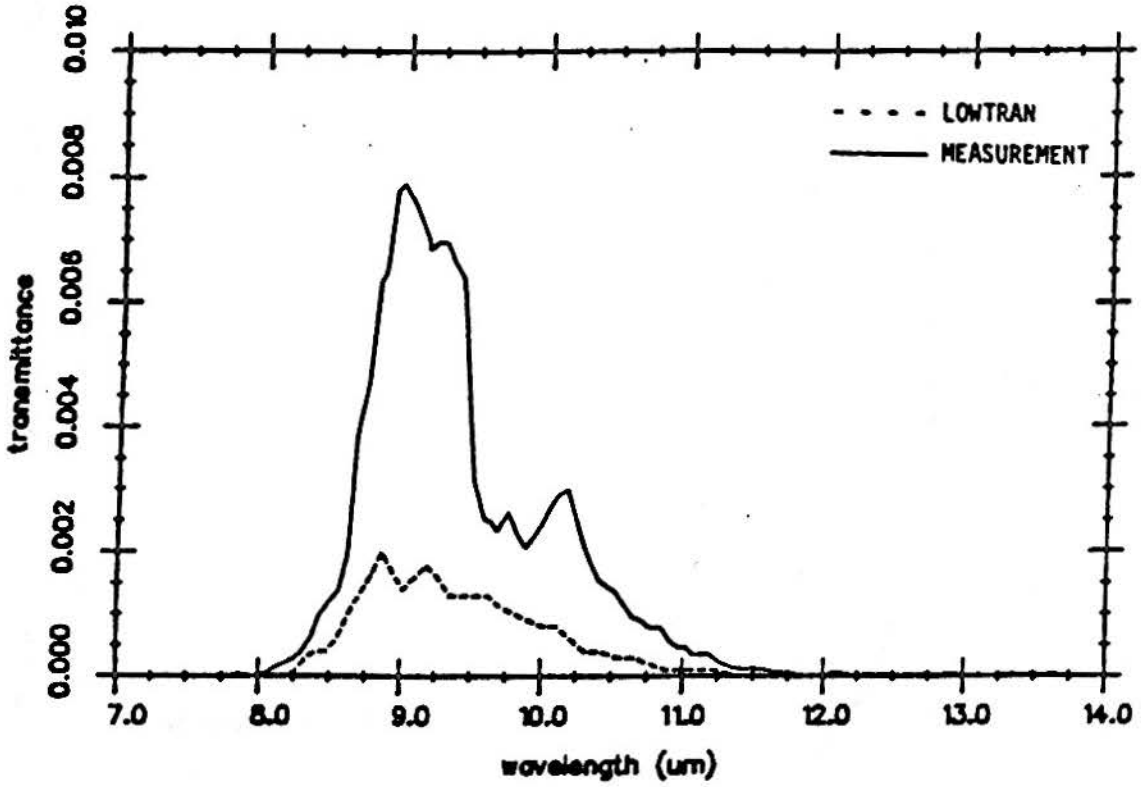


(a)

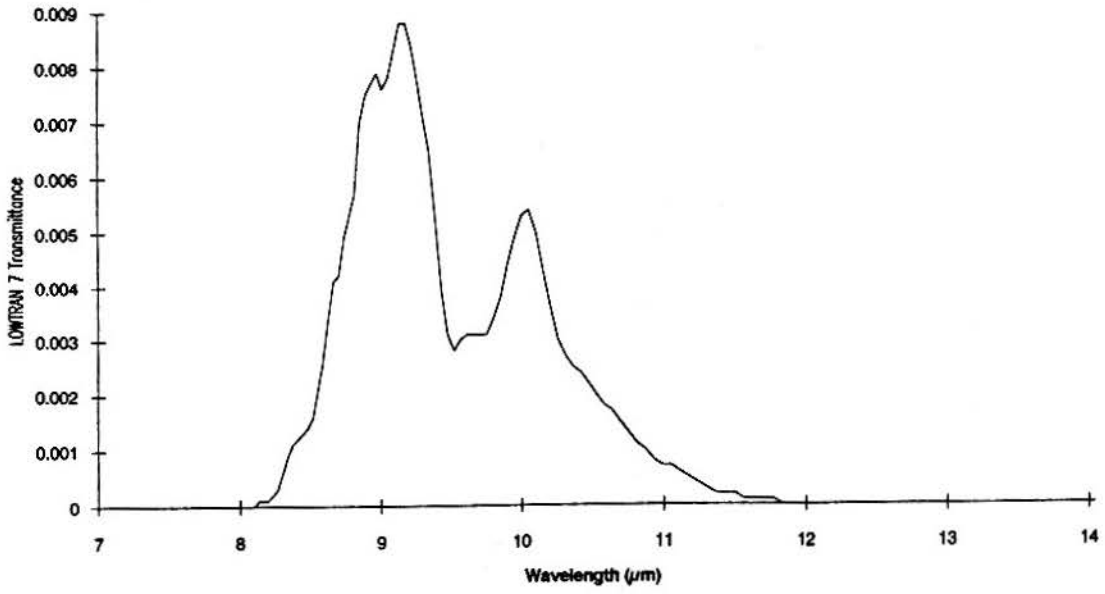


(b)

**Figure 26. Atmospheric Transmission over 66.2 km Path with the Radiosonde Profiles of Figure 27 (7-14 $\mu$m).**

**(a) Measured and LOWTRAN 6 curves from Manning et al[11]**

**(b) LOWTRAN 7 Navy Maritime Atmosphere 100 km Visibility**

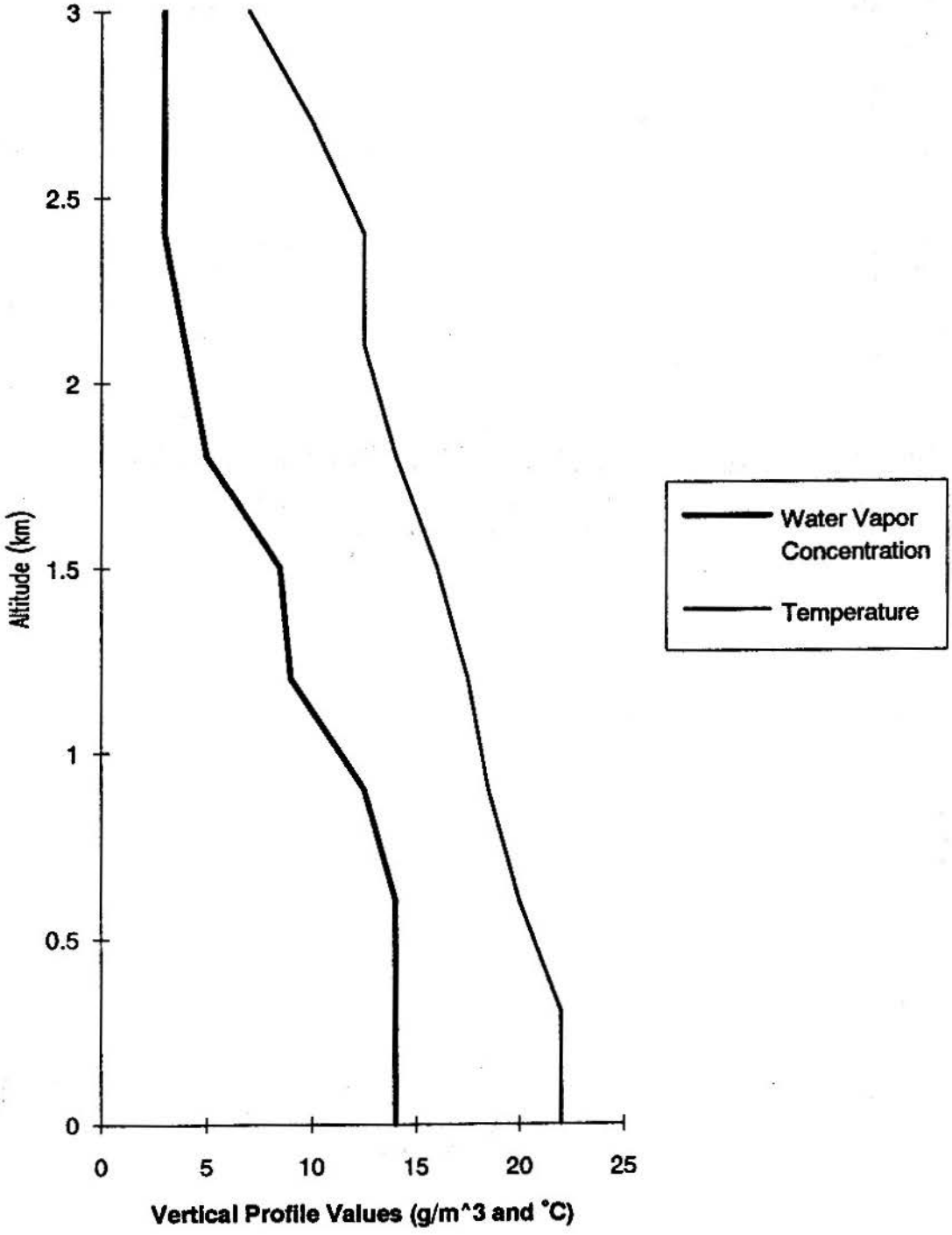


**Figure 27. Measured Radiosonde Profiles for Figures 25, 26, and 28.**

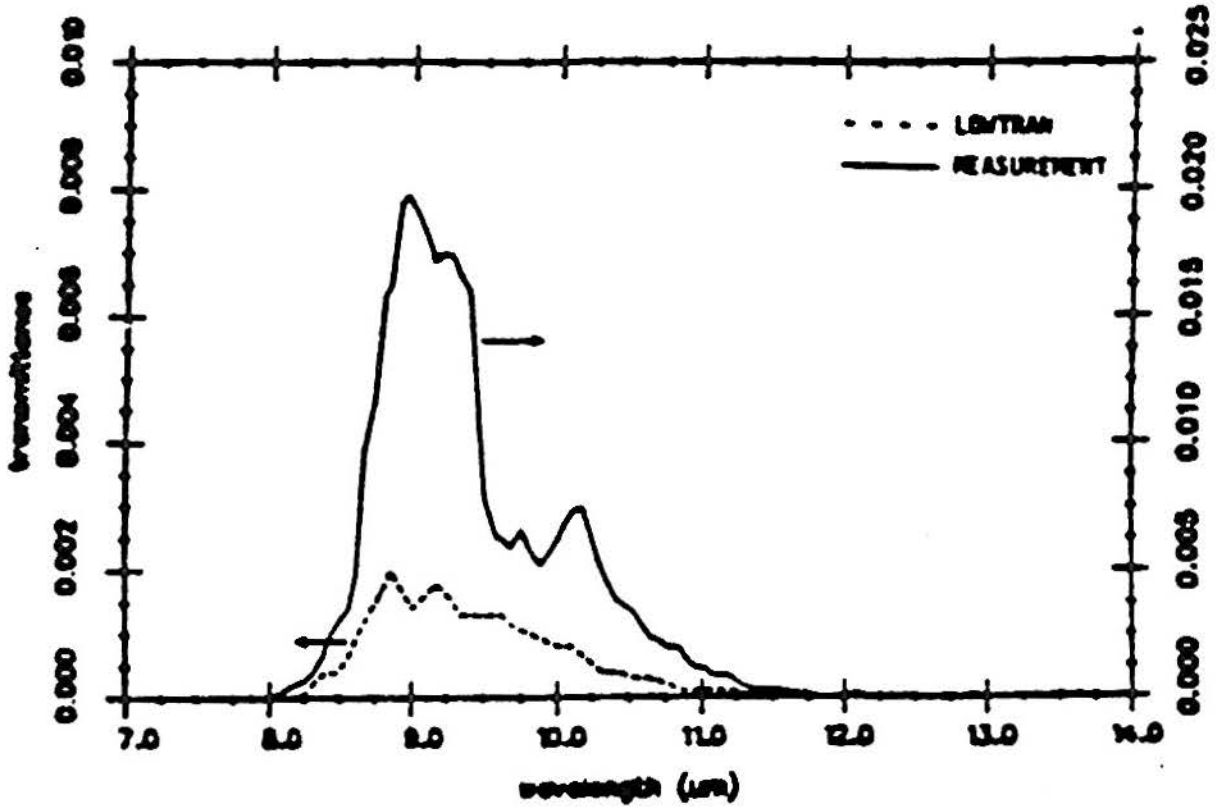


(a)

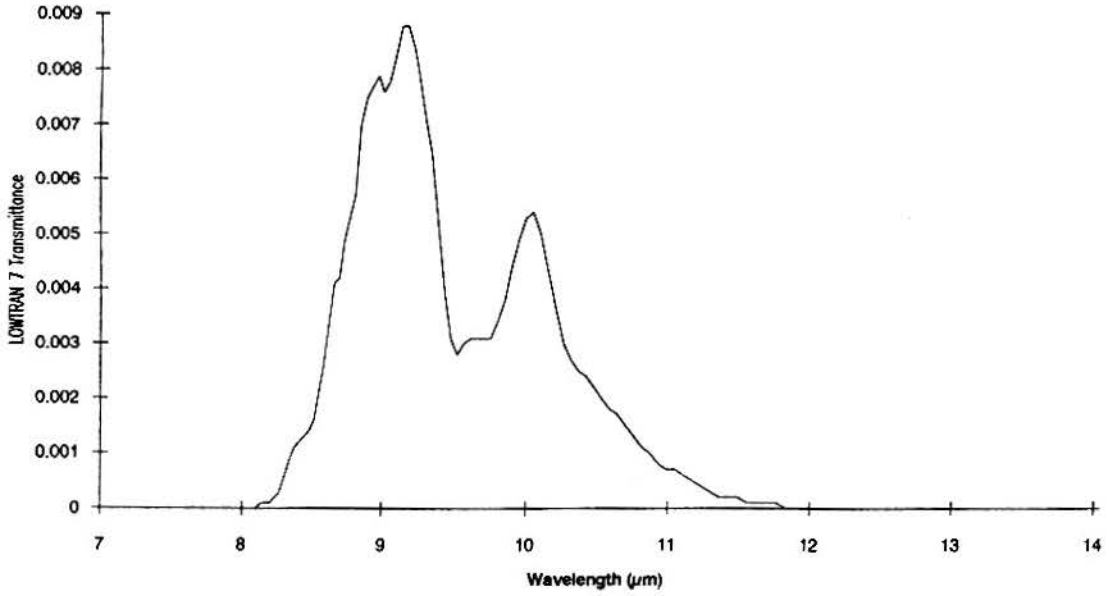


(b)

**Figure 28. Atmospheric Transmission over 66.2 km Path with the Radiosonde Profiles of Figure 27 (7-14 $\mu$m).**

**(a) Measured and LOWTRAN 6 curves from Hess et al[12]**

**(b) LOWTRAN 7 Navy Maritime Atmosphere 100 km Visibility**